

REGULAR PAPER

Scattering of e^\pm from the neon isonuclear series over the energy range 1 eV–0.5 GeV

To cite this article: Mahmudul H. Khandker *et al* 2020 *Jpn. J. Appl. Phys.* **59** SHHA05

View the [article online](#) for updates and enhancements.

You may also like

- [Theoretical calculations for precision polarimetry based on Mott scattering](#)
X. Roca-Maza
- [\$e^\pm\$ Ar scattering in the energy range 1 eV–E, 0.5 GeV](#)
M M Haque, A K F Haque, D H Jakubassa-Amundsen *et al.*
- [Spin-dependent electron reflection at W\(110\)](#)
C Angrick, J Braun, H Ebert *et al.*



Scattering of e^\pm from the neon isonuclear series over the energy range 1 eV–0.5 GeV

Mahmudul H. Khandker¹ , A. K. F. Haque^{1,2,3*} , M. Maaza^{2,3}, and M. Alfaz Uddin¹

¹Atomic and Molecular Physics Lab, Department of Physics, University of Rajshahi, Rajshahi-6205, Bangladesh

²Nanosciences African network (NANOAFNET), Materials Research Group (MRG), iThemba LABS-National Research Foundation (NRF), 1 Old Faure Road, 7129, PO Box 722, Somerset West, Western Cape Province, South Africa

³UNESCO-UNISA Africa Chair in Nanosciences/Nanotechnology Laboratories, College of Graduate Studies, University of South Africa (UNISA), Muckleneuk Ridge, PO Box 392, Pretoria, South Africa

*E-mail: fhaque@ru.ac.bd

Received October 30, 2019; revised December 19, 2019; accepted February 10, 2020; published online March 5, 2020

This work calculates the differential, integral and momentum transfer cross sections for the scattering of e^\pm by the neutral neon over the energy range 1 eV–0.5 GeV and those of e^- by the ions ($\text{Ne}^+ - \text{Ne}^{10+}$) over the range 1 eV–1 keV. It also includes the estimation of the viscosity, inelastic, total and total ionization cross sections and Sherman function for the e^\pm -atom systems over the same energy range. Our calculations involve two approaches, the optical potential model (OPM) and the nuclear structure approach (NSA), depending upon the collision energy. Both the approaches employ Dirac partial wave analysis but differ in the potentials. In OPM, a complex projectile-target optical potential, comprising static, exchange, polarization and imaginary components, is employed. In the NSA, only the nuclear potential is used, neglecting the screening of the electrons. Moreover, we have determined positions of critical minima, in energy and angle, from the analysis of elastic differential cross sections and Sherman function at different energies. Our results agree reasonably well with the available experimental data and other theoretical calculations. © 2020 The Japan Society of Applied Physics

1. Introduction

Experimental and theoretical studies on angular differential scattering (DCS), Integrated elastic (IECS), momentum transfer (MTCS), viscosity (VICS), Inelastic (INCS), total (TCS) and total ionization (TICS) cross-sections for the scattering of electron and positron by atoms and ions are of considerable continuing interest to both experimental and theoretical physicists because of their importance in understanding projectile-target interaction, the structure of matter and collision dynamics. The scattering observables have applications in surface analysis technique, electron microscopy, electron-probe microanalysis, design of radiation detectors, radiation therapy and protection, astrophysics, atmospheric sciences, biological sciences, gas discharges, plasma physics, X-ray lasers, etc.^{1–4} Determination of critical minima (CM) in DCSs, in the vicinity of which the maximum polarization occurs,⁵ is used in testing fundamental predictions of quantum mechanics. Polarized beams of electrons are applied in the transfer of polarization from electrons to photons.⁶

The earlier investigations of CM in the DCSs of electrons have been confined to heavy atoms and high incident energies of the projectile. Recently works on the studies of CM and spin polarization have been reported for light atoms and low energies.^{7–9}

The literature is rife with experimental studies on the scattering of electron by neon atom. DCSs for electron scattering have been measured by Gulley et al.¹⁰ (0.75–7 eV); Brewer et al.¹¹ (7.5–20 eV); Register and Trajmar et al.¹² (5–100 eV); Williams and Crowe¹³ (20–200 eV); Bromberg¹⁴ (200–700 eV); DuBois and Rudd¹⁵ (50–800 eV); Gupta and Rees¹⁶ (100–625 eV) and Jansen et al.¹⁷ (100–3000 eV). DCSs for positron scattering at few energies have been reported by Kauppila et al.¹⁸ Knight et al.¹⁹ and Kauppila et al.¹⁸ measured the energy variation of DCS for electron scattering and positron scattering respectively. For electron scattering, there have been measurements of experimental data by

de Heer et al.²⁰ Jansen et al.¹⁷ Gulley et al.¹⁰ and Williams and Crowe¹³ for IECSs; by Register and Trajmar¹² and Robertson²¹ for MTCs; by Nickel et al.²² Zecca et al.²³ Wagenaar et al.²⁴ Garcia et al.²⁵ and Salop et al.²⁶ for TCSs. For positron scattering, Bransden et al.²⁷ Griffith et al.²⁸ Kauppila et al.²⁹ and Jones et al.³⁰ published the TCSs data.

There are also theoretical studies on electron and positron scattering from neon atom as follows. Saha³¹ predicted low energy electron scattering of neon using the configuration-interaction procedure by taking into account the dynamical polarization and electron-correlation effects. McEachran and Stauffer³² examined the effects of polarization potential and exchange potentials in the adiabatic exchange approximation for the low incident energies. Fon and Berrington³³ investigated the scattering of slow electrons by neon in the elastic channel using R-matrix calculations. Byron et al.³⁴ used a full wave treatment of pseudo-potential derived from eikonal-Born series method within the framework of optical model formalism to explain elastic scattering of electron and positron at intermediate energies. Riley et al.³⁵ presented the scattering of fast electrons by neon using relativistic static approximation with nonrelativistic atomic wave functions. Baluja et al.³⁶ calculated DCSs for positron scattering using optical potential approach within the partial wave analysis method using a position correlation polarization and semi empirical absorption potential.

Positronium formation takes place at low and intermediate energies as a result of interaction of the positron with the bound electrons of the target³⁷ in positron-atom scattering. Treatment of this process is very complicated and can be tackled using coupled channel, quantum electrodynamics, R-matrix and many-body theories. Positron and electron annihilate to create photons. This can happen from direct interaction of the positron with the bound electrons and also from the excited state of the positronium. The OPM and NSA methods lack the option of the treatment of the positronium formation and annihilation.

Comparative investigations on electron and positron scattering at energies in the MeV or GeV region are scarce, particularly for the data of spin asymmetry.³⁸⁾ Not a single article studies all the features of lepton-Ne scattering over a broad energy domain up to the order of GeV. So the scope and usefulness of the study of this scattering covering the all-out features up to GeV order still remain. Moreover, testing a different procedure of production of data for this system might be another interesting point of investigation. Following the reasonable success of our previous works,^{2,39)} within the framework of Dirac Partial wave analysis, a complex atomic OPM is employed to calculate DCSs, IECSs, MTCSs, VICSs, INCSs and TCSs for the scattering of electron and positron in the energy range 1 eV–10 keV. We have extended our calculations of the energy variation of the DCSs and the Sherman function up to energies of the order of GeV, using the NSA.⁴⁰⁾ This work also presents the theoretical investigation of the elastic scattering of all the ions of neon isonuclear series in an objective of getting insight into the ionic charge and energy dependence of various cross-sections of the ions. For the electron-ion scattering, this work uses a short range electron-ion optical potential arising from the interaction of the projectile with the bound electrons and nucleus in conjunction with the pure form of long range Coulomb field due to the net ionic charge.

In OPM, the potential has both real and imaginary parts. The real part consists of a static potential,⁴¹⁾ exchange potential (used only for electron scattering)⁴²⁾ and a correlation-polarization potential.⁴³⁾ Static potential is generated from the electrostatic interactions of the projectile electron or positron with the target electrons and protons, using the analytical electron density given by Koga⁴⁴⁾ and Fermi nuclear charge distribution. Since the projectile electron exchanges places with a target electron, the exchange potential is required to account this rearrangement during scattering.⁴²⁾ Exchange potential is omitted for positron scattering because there is no exchange between the positron and bound electrons. Correlation-polarization potential combines the Buckingham long-range polarization potential with the correlation potential of Perdew and Zunger⁴⁵⁾ for electron and of Jain⁴⁶⁾ for positron. When the incident energy of the projectile is above the first excitation threshold, there is a loss of the incident flux to the inelastic channels. This loss is described by a negative imaginary potential which is obtained from the local density approximation (LDA), using the Born–Ochkur approximation and the Lindhard dielectric function.^{47,48)}

For high incident energies, the projectile gets close to the nucleus where the screening effect of electrons is negligible, thereby making the nuclear potential dominant for scattering. At energies above 10 MeV, magnetic scattering arises for nuclei with spin due to the current–current interaction between charged particles.⁴⁹⁾ The distorted-wave Born approximation, also based on the decomposition of the scattering states into partial waves, is applied to describe this magnetic scattering.³⁸⁾ In the present work, any magnetic scattering is absent because the ²⁰Ne nucleus has zero spin. We show that our OPM and NSA methods establish a bridge between the low energy and high energy results.

In this paper, we calculate DCSs for the scattering of electrons from neutral neon over the energy range

3.4 eV–10 keV and from neon ions (Ne⁺–Ne¹⁰⁺) over the range 10–100 eV. Due to lack of available experimental data, we chose a comparatively short energy range 13.6 eV–300 eV for positron scattering. We present the calculations of energy variation of DCSs in the energy range 1 eV–0.5 GeV at 50°, 90° and 130° for electron and at 60°, 90° and 120° for positron. We obtain CM in DCSs for electron scattering analyzing the Sherman function and DCSs and compare with available experimental results and theoretical predictions. We compare our calculations for IECS, MTCS, VICS, INCS and TCS for both electron and positron in the energy range 1 eV–10 keV with the available experimental data and theoretical calculations. We also present the calculations of IECS and MTCS for the scattering of *e*[−] off all the ions of neon isonuclear series.

The paper is organized as follows. The outline of the theory is given in Sect. 2. In Sect. 3, we provide the discussions of our DCS, CM, IECS, MTCS, VICS, INCS, TCS and TICS in comparison with other calculations and measurements. The Sect. 4 contains the conclusion of our findings.

2. Theory

As mentioned above, a complex optical potential within the framework of relativistic partial wave analysis is used to calculate different cross sections.

2.1. Optical potential

The complex optical potential used for the electron atom scattering calculations has the following form:

$$V(r) = V_{\text{st}}(r) + V_{\text{ex}}(r) + V_{\text{cp}}(r) - iW_{\text{abs}}(r). \quad (1)$$

Here, $V_{\text{st}}(r)$, $V_{\text{ex}}(r)$ and $V_{\text{cp}}(r)$, the components of the real part of OPM, represent the static, exchange and correlation-polarization potentials respectively and the imaginary part, W_{abs} represents the absorption potential. For positron, V_{ex} in $V(r)$ is omitted as exchange does not arise due to distinguishability of the projectile positron and bound electrons.

For the electron ion scattering, OPM is represented by a modified Coulomb potential given as

$$V(r) = \frac{qe^2}{r} + V_{\text{sr}}(r), \quad (2)$$

where q is the ionic charge and $V_{\text{sr}}(r)$ is a short range potential that vanishes at $r > r_{\text{c}}$. $V_{\text{sr}}(r)$ has the form of Eq. (1).

In case of unscreened nuclei, the scattering reduces to pure Coulomb scattering and Eq. (2) can then be written as

$$V(r) = \frac{qe^2}{r}. \quad (3)$$

2.1.1. Static potential. Considering the target as a frozen distribution of charge, elastic scattering of electrons and positrons is described by means of static field approximation. Within this approximation, interaction potential is completely determined by the nuclear and electronic charge distributions. Fermi nuclear charge distribution and analytical electron density given by Koga⁴⁴⁾ are used in the present calculations. The potential energy of the projectile at a distance r from the nucleus of the target atom is given by

$$V_{st}(r) = Z_0 e \varphi(r) = Z_0 e [\varphi_e(r) + \phi_n(r)], \quad (4)$$

where Z_{0e} is the projectile charge ($Z_0 = -1$ for electrons and $+1$ for positrons) and $\varphi_n(r)$ and $\varphi_e(r)$ are given by

$$\varphi_n(r) = e \left(\frac{1}{r} \int_0^r \varrho_n(r') 4\pi r'^2 dr' + \int_r^\infty \varrho_n(r') 4\pi r' dr' \right) \quad (5)$$

And

$$\varphi_e(r) = -e \left(\frac{1}{r} \int_0^r \varrho_e(r') 4\pi r'^2 dr' + \int_r^\infty \varrho_e(r') 4\pi r' dr' \right). \quad (6)$$

Here, $\varrho_n(r)$ and $\varrho_e(r)$ are respectively the space densities of protons and orbital electrons.¹⁾ For a neutral target atom with atomic number Z , proton and electron density functions $\varrho_n(r)$ and $\varrho_e(r)$ are normalized to Z as given by the following equation

$$\int \varrho(r) 4\pi r^2 dr = Z. \quad (7)$$

The electron density function is renormalized to the number of ionic electrons in case of ion.

2.1.2. Exchange potential. For electron scattering, an exchange potential is needed due to the indistinguishability of the projectile and the target electrons. The exchange potential is non-local. It is approximated by a local potential for an easy but accurate solution of the Dirac equation, as the exchange potential is negligible at high energies.⁴²⁾ In the present work, we use the semi-classical exchange potential of Furness and McCarthy.⁵⁰⁾ This is obtained from the non-local exchange interaction using the WKB like wave function. This potential is given as

$$V_{ex}(r) = \frac{1}{2} [E_i - V_{st}(r)] - \frac{1}{2} \{ [E_i - V_{st}(r)]^2 + 4\pi a_0 e^4 \varrho_e(r) \}^{1/2}. \quad (8)$$

Here, E_i is the impact energy of the electron and a_0 is the Bohr radius.

2.1.3. Correlation-polarization potential. The incident projectile, electron or positron, causes polarization of the target, thereby inducing electric field that attracts the projectiles. The asymptotic form of the polarization potential as given by Buckingham is

$$V_{cp,B}(r) = -\frac{\alpha_d e^2}{2(r^2 + d^2)^2}, \quad (9)$$

where α_d is the dipole polarizability of the target atom and d is the phenomenological cut-off parameter which is introduced to avoid singularity at the $r=0$. Mittleman and Watson⁵¹⁾ suggested

$$d^4 = \frac{1}{2} \alpha_d a_0 Z^{-1/3} b_{pol}^2, \quad (10)$$

Here, b_{pol} is an adjustable energy dependent parameter. In case of electron ion scattering, Z in Eq. (10) should be replaced by $(Z - q)$. Considering the fact that the magnitude of the polarization effects decreases as the projectile energy increases, Seltzer⁴⁷⁾ suggested the following empirical formula:

$$b_{pol}^2 = \max\{(E - 50 \text{ eV}) / (16 \text{ eV}), 1\}. \quad (11)$$

The charge of the projectile is dynamically screened by atomic electrons during its penetration through the bulk of the atom. In case of electron projectile, bound electrons get repelled and form a “Coulomb hole” surrounding the projectile from which other electrons are expelled. This effect is referred to as “correlation”. In LDA, the correlation energy of the projectile at r is taken as the same as if it were moving within a free electron gas (FEG) of density ϱ equal to the local atomic electron density. Following Padial and Norcross⁴³⁾ the short range correlation potential is calculated as the functional derivative of the FEG correlation energy with respect to ϱ . It is convenient to introduce the density parameter

$$r_s \equiv \frac{1}{a_0} \left[\frac{3}{4\pi \varrho_e(r)} \right]^{1/3}. \quad (12)$$

For electrons, Perdew and Zunger⁴⁵⁾ gave the following analytic form for the following correlation potential

$$V_{co}^{(-)}(r) = -\frac{e^2}{a_0} (0.0311 \ln r_s - 0.0584 + 0.00133 r_s \ln r_s - 0.0084 r_s), \quad \text{for } r_s < 1 \quad (13)$$

and

$$V_{co}(r) = -\frac{e^2}{a_0} \beta_0 \frac{1 + (7/6)\beta_1 r_s^{1/2} + (4/3)\beta_2 r_s}{(1 + \beta_1 r_s^{1/2} + \beta_2 r_s)^2}, \quad \text{for } r_s \geq 1, \quad (14)$$

where $\beta_0 = 0.1423$, $\beta_1 = 1.0529$ and $\beta_2 = 0.3334$.

For positrons, the correlation potential as given by Jain⁴⁶⁾ is

$$V_{co}^{(+)}(r) = \frac{e^2}{2a_0} \{ -1.82 r_s^{-1/2} + [0.051 \ln(r_s) - 0.115] \times \ln(r_s) + 1.167 \}, \quad \text{for } r_s < 0.302, \quad (15)$$

$$V_{co}^{(+)}(r) = \frac{e^2}{2a_0} [-0.92305 - 0.09098 r_s^{-2}] \quad (16)$$

for $0.302 \leq r_s < 0.56$,

and

$$V_{co}^{(+)}(r) = \frac{e^2}{2a_0} \left[-\frac{8.7674}{(r_s + 2.5)^3} + \frac{-13.151 + 0.9552 r_s}{(r_s + 2.5)^2} + \frac{2.8655}{(r_s + 2.5)} - 0.6298 \right] \quad \text{for } 0.56 \leq r_s < 8.0. \quad (17)$$

For the asymptotic region, $8.0 \leq r_s \leq \infty$, the polarization potential is accurately given by the Buckingham potential.

The global correlation-polarization potential is determined by combining the long range Buckingham potential with the short range LDA correlation potential as follows⁴⁷⁾

$$V_{\text{cp}}^{\pm}(r) \equiv \begin{cases} \max\{V_{\text{co}}^{\pm}(r), V_{\text{cp},B}(r)\} & \text{if } r < r_{\text{cp}} \\ V_{\text{cp},B}(r) & \text{if } r \geq r_{\text{cp}} \end{cases} \quad (18)$$

Here, r_{cp} is the outer radius at which $V_{\text{co}}^{\pm}(r)$ and $V_{\text{pol}}(r)$ cross first.

2.1.4. Absorption potential. When the kinetic energy of the projectiles is above the first excitation threshold, there is a depletion of the elastically scattered electrons. This depletion causes a reduction in elastic DCS at intermediate and large angles.¹⁾ To account for this effect, a negative imaginary term, $-iW_{\text{abs}}(r)$ is included in the optical potential. In the approach of LDA, the projectile interacts as if it were moving within a homogeneous electrons gas of density $\rho_e(r)$ with velocity⁴⁷⁾

$$v_L^{(\text{nr})} = \left(\frac{2E_L}{m_e} \right)^{1/2} \quad (19)$$

corresponding to the local kinetic energy

$$E_L(r) = \begin{cases} E_i - V_{\text{st}}(r) - V_{\text{ex}}(r) & \text{for electron} \\ \max\{E_i - V_{\text{st}}, 0\} & \text{for positron.} \end{cases} \quad (20)$$

Assuming that the interactions with the electron gas are binary collisions, the absorption probability per unit time can be written as

$$\frac{2}{\hbar} W_{\text{abs}}^{(\text{nr})}(r) = A_{\text{abs}} [v_L^{(\text{nr})} \rho_e(r) \sigma_{\text{bc}}(E_L, \rho_e, \Delta)]. \quad (21)$$

where A_{abs} is an empirical parameter that takes values of the order unity and $\sigma_{\text{bc}}(E_L, \rho, \Delta)$ is the non-relativistic Born approximated cross section for collisions involving energy transfer greater than a certain energy gap Δ .⁴⁷⁾ The value of the energy gap Δ in this calculation is adopted as

$$\Delta = \begin{cases} \epsilon_1 & \text{for electron,} \\ \max\{I - 6.8 \text{ eV}, 0\} & \text{for positron.} \end{cases} \quad (22)$$

Here, ϵ_1 and I are respectively the first excitation energy and ionization potential of atom. The quantity 6.8 eV is the positronium binding energy. Since the effect of inelastic absorption is appreciable up to relatively high energies, the non-relativistic expression (18) needs to be modified to account for the relativistic effects. The relativistic velocity can be introduced as

$$v_L(r) = c \sqrt{\frac{E_L(E_L + 2m_e c^2)}{(E_L + m_e c^2)^2}}. \quad (23)$$

This correction leads to the “semi-relativistic” absorption potential

$$W_{\text{abs}}(r) \equiv \frac{v_L^{(\text{nr})}}{v_L} W_{\text{abs}}^{(\text{nr})}(r) = \sqrt{\frac{2(E_L + m_e c^2)^2}{m_e c^2 (E_L + 2m_e c^2)}} \times A_{\text{abs}} \frac{\hbar}{2} [v_L^{(\text{nr})} \rho_e(r) \sigma_{\text{bc}}(E_L, \rho_e, \Delta)]. \quad (24)$$

The inclusion of relativistic effects causes the absorption potential to approach a saturation value with the increase of E_i . In the present calculations, the value of the parameter A_{abs} is taken as 2 for electron and 4 for positron scattering. A_{abs} is an adjustable parameter and its value depends on the

projectile-atom combination. In case of TICS calculations, it is taken as 4.

2.2. Dirac partial wave analysis

The scattering of electrons and positrons by a central field $V(r)$ is completely described by the direct and spin flip scattering amplitudes given by^{8,52)}

$$f(\theta) = \frac{1}{2ik} \sum_{\ell=0}^{\infty} \{(\ell+1)[\exp(2i\delta_{\kappa=-\ell-1}) - 1] + \ell[\exp(2i\delta_{\kappa=\ell}) - 1]\} P_{\ell}(\cos \theta) \quad (25)$$

and

$$g(\theta) = \frac{1}{2ik} \sum_{\ell=0}^{\infty} [\exp(2i\delta_{\kappa=\ell}) - \exp(2i\delta_{\kappa=-\ell-1})] P_{\ell}^1(\cos \theta) \quad (26)$$

respectively. k , the relativistic wave number of the projectile, is related to the kinetic energy E_i by

$$(c\hbar k)^2 = E_i(E_i + 2m_e c^2), \quad (27)$$

where c is the velocity of light in vacuum. $P_{\ell}(\cos \theta)$ and $P_{\ell}^1(\cos \theta)$ are the Legendre polynomials and associated Legendre functions respectively. The total relativistic wave function, with quantum numbers κm , which describe the motion of the scattered projectile is given by

$$\psi_{E\kappa m}(\vec{r}) = \frac{1}{r} \begin{pmatrix} P_{E\kappa}(r) \Omega_{\kappa, m}(\hat{r}) \\ iQ_{E\kappa}(r) \Omega_{-\kappa, m}(\hat{r}) \end{pmatrix}. \quad (28)$$

Here, $P_{E\kappa}(r)$ and $Q_{E\kappa}(r)$ represent respectively the radial parts of the large and small components of the scattering wave function and $\Omega_{\kappa, m}(\hat{r})$ are the spherical spinors. The relativistic quantum number κ is defined as $\kappa = (\ell - j)(2j + 1)$, where j and ℓ are the total and orbital angular momentum quantum numbers that are both determined by the value of κ as $j = |\kappa| - 1/2$, $\ell = j + \kappa/(2|\kappa|)$. $P_{E\kappa}(r)$ and $Q_{E\kappa}(r)$, respectively satisfy the following set of coupled differential equations⁵³⁾

$$\frac{dP_{E\kappa}}{dr} = -\frac{\kappa}{r} P_{E\kappa}(r) + \frac{E_i - V + 2m_e c^2}{c\hbar} Q_{E\kappa}(r) \quad (29)$$

and

$$\frac{dQ_{E\kappa}}{dr} = -\frac{E_i - V}{c\hbar} P_{E\kappa}(r) + \frac{\kappa}{r} Q_{E\kappa}(r). \quad (30)$$

Various scattering cross sections are determined from the asymptotic form of the large component $P_{E\kappa}(r)$ of the scattering wave function which can be expressed in terms of the complex phase-shift δ_{κ} as

$$P_{E\kappa}(r) \simeq \sin\left(kr - \ell\frac{\pi}{2} + \delta_{\kappa}\right). \quad (31)$$

The Eqs. (29) and (30) satisfying the asymptotic condition (31) are solved numerically using the subroutine package RADIAL.⁵⁴⁾ Once the phase shifts and the scattering amplitudes are determined, the elastic differential cross section is obtained from the expression

$$\frac{d\sigma}{d\Omega} = |f(\theta)|^2 + |g(\theta)|^2. \quad (32)$$

The degree of spin polarization of the electrons or positrons from an initially unpolarized beam that are scattered in the direction θ is given by Sherman function⁵⁵⁾

$$S(\theta) \equiv i \frac{f(\theta)g^*(\theta) - f^*(\theta)g(\theta)}{|f(\theta)|^2 + |g(\theta)|^2}. \quad (33)$$

The total integrated elastic σ_{el} , the momentum transfer σ_m and viscosity σ_v cross sections are expressed in terms of the scattering amplitudes $f(\theta)$ and $g(\theta)$ as

$$\sigma_{\text{el}} = \int \frac{d\sigma}{d\Omega} d\Omega = 2\pi \int_0^\pi (|f(\theta)|^2 + |g(\theta)|^2) \sin(\theta) d\theta, \quad (34)$$

$$\sigma_m = 2\pi \int_0^\pi (1 - \cos \theta) (|f(\theta)|^2 + |g(\theta)|^2) \sin(\theta) d\theta, \quad (35)$$

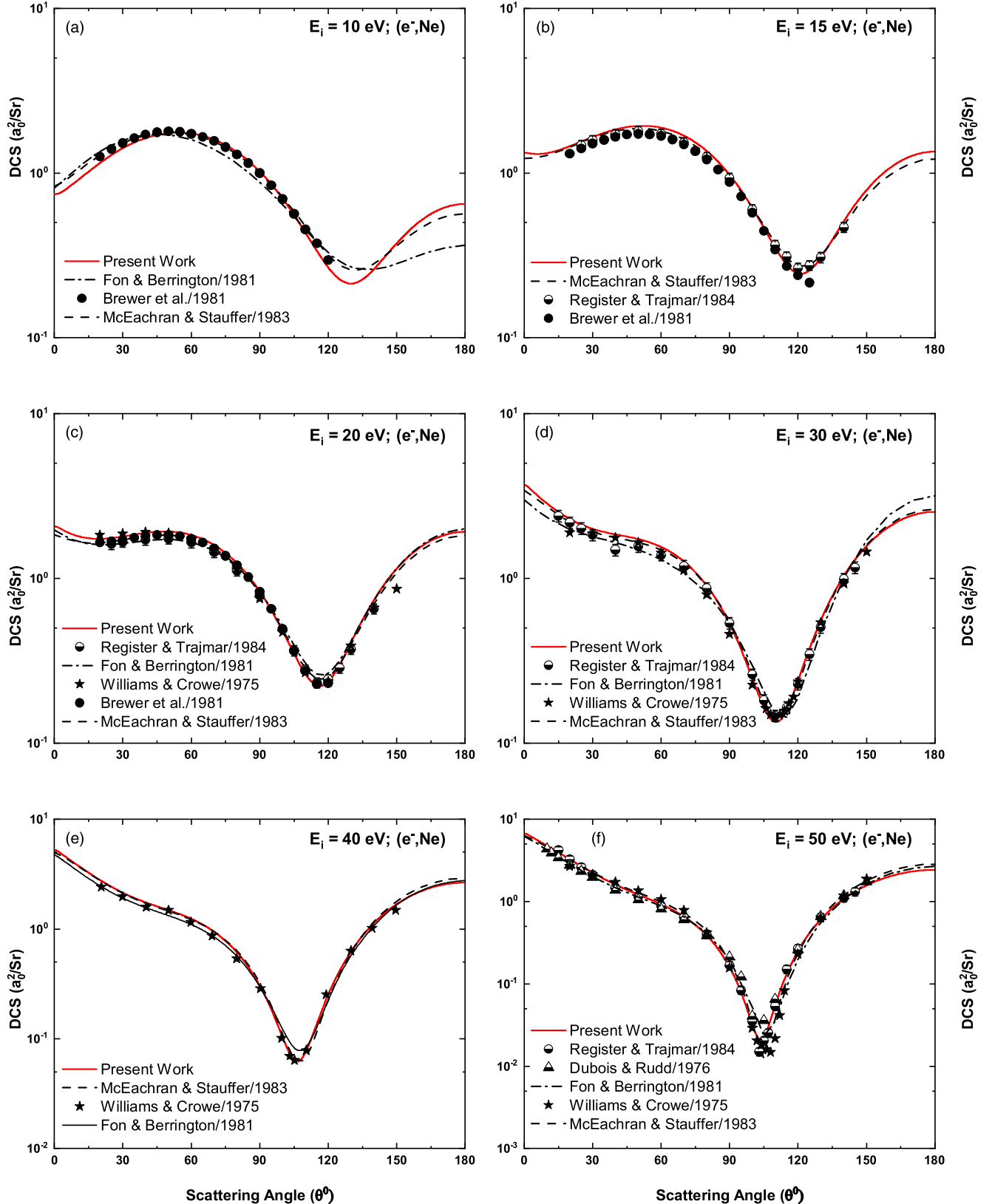


Fig. 1. (Color online) DCS (a_0^2/Sr) for elastic e^- –Ne scattering at energies 10, 15, 20, 30, 40 and 50 eV. Theoretical: McEachran and Stauffer³²⁾ Fon and Berrington.³³⁾ Experimental: Brewer et al.¹¹⁾ and Register and Trajmar,¹²⁾ Williams and Crowe¹³⁾ and DuBois and Rudd.¹⁵⁾

Table I. DCS (a_0^2/Sr) for elastic $e^- - \text{Ne}$ scattering at energies 3.4, 4.2, 5.0, 7.0, 7.5 and 10 eV, Experimental (Exp.) reference(s): Gulley et al.^[10] and Brewer et al.^[11]

θ	3.4 eV		4.2 eV		5.0 eV		7.0 eV		7.5 eV		10 eV	
	OPM	Exp. ^[10]	OPM	Exp. ^[10]	OPM	Exp. ^[10]	OPM	Exp. ^[10]	OPM	Exp. ^[11]	OPM	Exp. ^[11]
0	0.1273		0.2089		0.2876		0.4694		0.5134		0.7443	
2	0.1316		0.2153		0.2959		0.4806		0.5248		0.7539	
4	0.1441		0.2336		0.3192		0.5113		0.5561		0.7807	
6	0.1634		0.2610		0.3531		0.5536		0.5989		0.8174	
8	0.1871		0.2931		0.3916		0.5992		0.6446		0.8569	
10	0.2128		0.3265		0.4305		0.6448		0.6906		0.8992	
12	0.2387		0.3595		0.4690		0.6918		0.7387		0.9459	
15	0.2774	0.5968	0.4095	0.6790	0.5286	0.7933	0.7667	0.9077	0.8154		1.0200	
20	0.3448	0.6825	0.4969	0.7933	0.6317	0.8684	0.8932	1.0470	0.9450	1.170	1.1520	1.260
25	0.4132		0.5823	0.8684	0.7316	1.0041	1.0190	1.1542	1.0740	1.300	1.2870	1.400
30	0.4780	0.8326	0.6638	0.9434	0.8267	1.0399	1.1370	1.2400	1.1960	1.420	1.4170	1.520
35	0.5387		0.7375	1.0113	0.9115	1.1471	1.2420	1.3543	1.3050	1.520	1.5350	1.630
40	0.5919	0.9363	0.8013	1.0792	0.9842	1.1757	1.3310	1.4151	1.3970	1.600	1.6340	1.710
45	0.6366		0.8530	1.1256	1.0410	1.2328	1.3980	1.4294	1.4660	1.640	1.7080	1.770
50	0.6713	1.0220	0.8907	1.1221	1.0810	1.2793	1.4420	1.4758	1.5100	1.660	1.7520	1.790
55	0.6948		0.9137	1.1507	1.1030	1.2614	1.4590	1.4401	1.5260	1.650	1.7640	1.780
60	0.7072	1.0184	0.9211	1.1614	1.1050	1.2507	1.4500	1.4437	1.5150	1.610	1.7410	1.730
65	0.7079		0.9134	1.1042	1.0890	1.2043	1.4150	1.3829	1.4750	1.550	1.6840	1.660
70	0.6976	0.9791	0.8909	1.0792	1.0550	1.1685	1.3540	1.3186	1.4090	1.460	1.5950	1.570
75	0.6770		0.8550	1.0399	1.0040	1.1006	1.2720	1.2507	1.3200	1.360	1.4780	1.440
80	0.6470	0.8969	0.8076	0.9720	0.9396	1.0435	1.1720	1.1292	1.2120	1.240	1.3390	1.300
85	0.6092		0.7504	0.9220	0.8642	0.9613	1.0570	1.0399	1.0890	1.110	1.1840	1.150
90	0.5653	0.7790	0.6859	0.8326	0.7806	0.8719	0.9339	0.9220	0.9580	0.988	1.0200	1.000
95	0.5167		0.6168	0.7719	0.6925	0.7754	0.8070	0.8255	0.8234	0.852	0.8564	0.844
100	0.4655	0.6647	0.5454	0.6897	0.6030	0.6933	0.6818	0.7075	0.6913	0.727	0.6996	0.696
105	0.4134		0.4742	0.6289	0.5152	0.6218	0.5632	0.6075	0.5670	0.609	0.5570	0.566
110	0.3619	0.5432	0.4056	0.5575	0.4322	0.5539	0.4553	0.5003	0.4551	0.504	0.4346	0.455
115	0.3125		0.3414	0.4860	0.3561	0.4824	0.3616	0.4217	0.3591	0.408	0.3370	0.375
120	0.2665	0.4324	0.2831	0.4252	0.2889	0.4252	0.2844	0.3645	0.2817	0.333	0.2671	0.296
125	0.2247		0.2318	0.3752	0.2317	0.3609	0.2252	0.2841	0.2241		0.2261	
130	0.1878	0.3459	0.1882	0.3288	0.1852	0.2973	0.1840	0.2487	0.1864		0.2133	
135	0.1560		0.1524		0.1492		0.1601		0.1675		0.2263	
140	0.1294		0.1242		0.1231		0.1515		0.1651		0.2612	
145	0.1079		0.1030		0.1058		0.1555		0.1763		0.3129	
150	0.0909		0.0878		0.0959		0.1691		0.1974		0.3755	
155	0.0780		0.0776		0.0915		0.1887		0.2243		0.4426	
160	0.0686		0.0713		0.0910		0.2108		0.2531		0.5080	
165	0.0621		0.0677		0.0927		0.2319		0.2800		0.5658	
170	0.0578		0.0660		0.0950		0.2492		0.3018		0.6110	
175	0.0554		0.0652		0.0969		0.2606		0.3159		0.6397	
180	0.0547		0.0650		0.0976		0.2645		0.3208		0.6496	

$$\sigma_v = 3\pi \int_0^\pi [1 - (\cos \theta)^2] (|f(\theta)|^2 + |g(\theta)|^2) \sin(\theta) d\theta. \quad (36)$$

The grand total cross section (TCS) σ_{tot} , sum of the total elastic (σ_{el}) and absorption cross section (σ_{inel}), is obtained by the following relation

$$\sigma_{\text{tot}} = \frac{4\pi}{k} \text{Im} f(0), \quad (37)$$

where Im denotes the imaginary part of the expression that follows and $f(0)$ stands for the scattering amplitude in the forward direction.

In case of electron ion scattering, $f(\theta)$ and $g(\theta)$ can be written as

$$f(\theta) = f_{\text{sr}}(\theta) + f^{(C)}(\theta), \quad g(\theta) = g_{\text{sr}}(\theta) + g^{(C)}(\theta). \quad (38)$$

Here $f^{(C)}(\theta)$ and $g^{(C)}(\theta)$, the scattering amplitudes for the Coulomb potential with $Z = q$, are given by

$$f^{(C)}(\theta) = \frac{1}{2ik} \sum_{\ell=0}^{\infty} \{(\ell+1)[\exp(2i\Delta_{-\ell-1}) - 1] + \ell[\exp(2i\Delta_{\ell}) - 1]\} P_{\ell}(\cos \theta) \quad (39)$$

and

$$g^{(C)}(\theta) = \frac{1}{2ik} \sum_{\ell=0}^{\infty} \{\exp(2i\Delta_{\ell}) - \exp(2i\Delta_{-\ell-1})\} P_{\ell}^1(\cos \theta). \quad (40)$$

And $f_{\text{sr}}(\theta)$ and $g_{\text{sr}}(\theta)$, the scattering amplitudes for the short range potential, are given as

$$f_{\text{sr}}(\theta) = \frac{1}{2ik} \sum_{\ell=0}^{\infty} \{(\ell+1)\exp(2i\Delta_{-\ell-1})[\exp(2i\hat{\delta}_{-\ell-1}) - 1] + \ell \exp(2i\Delta_{\ell})[\exp(2i\hat{\delta}_{\ell}) - 1]\} P_{\ell}(\cos \theta) \quad (41)$$

Table II. DCS (a_0^2/Sr) for the same as in Table I at energies 12.5, 15, 17.5, 20, 30 and 40 eV, Experimental reference(s): Brewer et al.^[11] Registrar & Trajmar^[12] and Williams & Crowe.^[13]

θ	12.5 eV		15 eV		17.5 eV		20 eV		30 eV		40 eV	
	OPM	Exp. ^[11]	OPM	Exp. ^[11]	OPM	Exp. ^[11]	OPM	Exp. ^[11]	OPM	Exp. ^[12]	OPM	Exp. ^[13]
0	1.0140		1.3290		1.6860		2.0710		3.6960		5.2500	
2	1.0160		1.3210		1.6630		2.0310		3.5680		5.0230	
4	1.0280		1.3100		1.6230		1.9590		3.3570		4.6810	
6	1.0480		1.3070		1.5930		1.9000		3.1730		4.3750	
8	1.0730		1.3110		1.5730		1.8520		3.0040		4.0900	
10	1.1030		1.3230		1.5610		1.8140		2.8530		3.8260	
12	1.1390		1.3400		1.5560		1.7850		2.7150		3.5840	
15	1.1980		1.3760		1.5620		1.7560		2.5360	2.3942	3.2540	
20	1.3120	1.260	1.4570	1.310	1.5990	1.550	1.7430	1.650	2.2970	2.1834	2.7900	2.3500
25	1.4350	1.400	1.5540	1.410	1.6600	1.610	1.7610	1.680	2.1230	2.0119	2.4210	
30	1.5580	1.500	1.6570	1.510	1.7340	1.690	1.8010	1.720	2.0010	1.8368	2.1350	1.9800
35	1.6710	1.620	1.7550	1.590	1.8100	1.760	1.8480	1.770	1.9160		1.9150	
40	1.7670	1.700	1.8400	1.660	1.8770	1.820	1.8920	1.820	1.8520	1.6831	1.7450	1.5500
45	1.8390	1.750	1.9020	1.710	1.9240	1.860	1.9210	1.840	1.7970		1.6070	
50	1.8790	1.780	1.9340	1.730	1.9440	1.870	1.9260	1.840	1.7350	1.5688	1.4850	1.4700
55	1.8840	1.770	1.9300	1.720	1.9290	1.850	1.8990	1.810	1.6560		1.3650	
60	1.8510	1.700	1.8870	1.680	1.8760	1.790	1.8350	1.740	1.5530	1.3865	1.2370	1.1600
65	1.7800	1.630	1.8050	1.600	1.7830	1.700	1.7330	1.650	1.4240		1.0960	
70	1.6740	1.590	1.6860	1.490	1.6540	1.580	1.5950	1.520	1.2680	1.1900	0.9424	0.8530
75	1.5380	1.450	1.5350	1.360	1.4930	1.430	1.4270	1.370	1.0910		0.7784	
80	1.3770	1.280	1.3600	1.210	1.3080	1.270	1.2370	1.200	0.9022		0.6112	0.5390
85	1.2000	1.120	1.1690	1.050	1.1100	1.090	1.0350	1.020	0.7111	0.8719	0.4499	
90	1.0170	1.010	0.9739	0.883	0.9094	0.898	0.8339	0.829	0.5301		0.3047	0.2820
95	0.8356	0.763	0.7847	0.721	0.7181	0.718	0.6449	0.654	0.3714	0.5360	0.1860	
100	0.6665	0.554	0.6119	0.574	0.5474	0.563	0.4802	0.492	0.2464		0.1032	0.1010
105	0.5178	0.525	0.4650	0.445	0.4074	0.426	0.3501	0.364	0.1650	0.2609	0.0643	
110	0.3965	0.402	0.3518	0.342	0.3062	0.325	0.2629	0.275	0.1345	0.1823	0.0748	0.0682
115	0.3078	0.315	0.2777	0.272	0.2494	0.263	0.2243	0.229	0.1593	0.1465	0.1377	
120	0.2548	0.262	0.2459	0.239	0.2400	0.249	0.2368	0.232	0.2403	0.1644	0.2527	0.2510
125	0.2383		0.2567	0.216	0.2778		0.2997		0.3755	0.2287	0.4169	
130	0.2569		0.3077		0.3598		0.4095		0.5591	0.3466	0.6243	0.6360
135	0.3068		0.3943		0.4801		0.5593		0.7828	0.5074	0.8663	
140	0.3825		0.5095		0.6306		0.7402		1.0360		1.1320	1.0200
145	0.4772		0.6446		0.8014		0.9410		1.3050	0.9899	1.4100	
150	0.5827		0.7898		0.9813		1.1500		1.5760	1.1650	1.6870	1.4900
155	0.6906		0.9351		1.1590		1.3540		1.8360		1.9480	
160	0.7927		1.0700		1.3220		1.5400		2.0710		2.1830	
165	0.8811		1.1860		1.4620		1.6990		2.2670		2.3790	
170	0.9494		1.2750		1.5680		1.8190		2.4160		2.5260	
175	0.9924		1.3310		1.6350		1.8950		2.5080		2.6170	
180	1.0070		1.3500		1.6580		1.9200		2.5400		2.6480	

and

$$g_{sr}(\theta) = \frac{1}{2ik} \sum_{l=0}^{\infty} \{ \exp(2i\Delta_l) [\exp(2i\hat{\delta}_l) - 1] - \exp(2i\Delta_{-l-1}) [\exp(2i\hat{\delta}_{-l-1}) - 1] \} P_l^1(\cos \theta). \quad (42)$$

Detail partial wave analysis for electron ion scattering is available at Khandker et al.^[56] In case of bare nucleus, the contributions to scattering amplitudes from V_{sr} become zero and $f(\theta)$ and $g(\theta)$ can be written as

$$f(\theta) = f^{(C)}(\theta), \quad g(\theta) = g^{(C)}(\theta). \quad (43)$$

The number of inner phase shifts in (41) and (42) was determined by the convergence criterion. The partial-wave series converge very slowly for the small angle elastic scattering by ions. To avoid this numerical instabilities in ELSEPA^[1] the calculations of scattering amplitudes and DCSs for ions is limited to scattering angles larger than $\sim 1^\circ$.

2.3. Ionization cross section

Total inelastic cross section σ_{inel} and Ionization cross section σ_{ion} satisfy the following relation

$$\sigma_{inel} \geq \sigma_{ion} \quad (44)$$

as the former itself is partitioned into excitation and ionization cross section. σ_{ion} can be calculated from the following energy dependent ratio as is done in^[57,58]

$$R(E_i) = \frac{\sigma_{ion}(E_i)}{\sigma_{inel}(E_i)}. \quad (45)$$

The ratio $R(E_i)$ is a continuous function of energy. For $E_i > I$ (ionization potential), this function is fitted to the equation

$$R(E_i) = 1 - A \left[\frac{B}{U + C} + \frac{\ln U}{U} \right], \quad (46)$$

where $U = E_i/I$ is the reduced energy. The adjustable parameters A , B and C are determined using the following conditions

Table III. DCS (a_0^2/Sr) for the same as in Table I at energies 50, 60, 65, 70, 80 and 90 eV, Experimental reference(s): Registrar and Trajmar.¹²⁾

θ	50 eV		60 eV		65 eV		70 eV		80 eV		90 eV
	OPM	Exp. ¹²⁾	OPM	Exp. ¹²⁾	OPM	Exp. ¹²⁾	OPM	Exp. ¹²⁾	OPM	Exp. ¹²⁾	OPM
0	6.7050		7.8480		8.3240		8.6990		9.3030		9.7760
2	6.3810		7.4330		7.8660		8.2020		8.7350		9.1440
4	5.9280		6.8820		7.2700		7.5690		8.0360		8.3850
6	5.5090		6.3660		6.7110		6.9750		7.3820		7.6780
8	5.1200		5.8840		6.1870		6.4170		6.7670		7.0150
10	4.7530		5.4300	7.2863	5.6940	7.9724	5.8920	7.9045	6.1880	7.1862	6.3910
12	4.4110		5.0030		5.2280		5.3970		5.6420		5.8010
15	3.9380	4.1845	4.4090	5.4745	4.5810	5.9069	4.7070	5.8033	4.8800	5.2851	4.9800
20	3.2530	3.2411	3.5400	4.3203	3.6330	4.4918	3.6960	4.2774	3.7630	3.9308	3.7760
25	2.6890	2.6051	2.8190		2.8480		2.8580		2.8390	2.8766	2.7880
30	2.2350	2.1012	2.2400	2.4728	2.2190	2.5050	2.1880	2.3978	2.1090	2.1083	2.0160
35	1.8790		1.7880		1.7320		1.6740		1.5560		1.4420
40	1.6030	1.4687	1.4450	1.6081	1.3670	1.5545	1.2920	1.4258	1.1550	1.1971	1.0350
45	1.3880		1.1870		1.0970		1.0150		0.8730		0.7581
50	1.2150	1.1399	0.9902	1.0435	0.8966	1.0399	0.8135	0.9005	0.6770	0.7361	0.5727
55	1.0650		0.8340		0.7422		0.6632		0.5380		0.4467
60	0.9270	0.8898	0.7016	0.7790	0.6157	0.6897	0.5437	0.6254	0.4333	0.4681	0.3559
65	0.7916		0.5815		0.5044		0.4413		0.3474		0.2837
70	0.6555	0.6432	0.4676	0.5539	0.4010	0.4717	0.3480	0.4113	0.2712	0.2970	0.2209
75	0.5192		0.3581		0.3032		0.2606		0.2009		0.1634
80	0.3867	0.4002	0.2550	0.2859	0.2120	0.2680	0.1798	0.2173	0.1366	0.1537	0.1111
85	0.2641		0.1623	0.2187	0.1311	0.1522	0.1086	0.1387	0.0806	0.1001	0.0665
90	0.1590	0.1680	0.0859	0.1072	0.0653	0.0797	0.0516	0.0783	0.0371	0.0515	0.0328
95	0.0791	0.0836	0.0317	0.0404	0.0202	0.0268	0.0138	0.0275	0.0103		0.0141
100	0.0316	0.0350	0.0054	0.0082	0.0010	0.0026	0.0000	0.0079	0.0045	0.0114	0.0137
105	0.0223	0.0204	0.0118	0.0065	0.0120	0.0158	0.0143	0.0134	0.0228		0.0343
110	0.0553	0.0536	0.0539	0.0504	0.0559	0.0647	0.0591	0.0475	0.0676	0.0640	0.0777
115	0.1325	0.1501	0.1331	0.1408	0.1342	0.1597	0.1355	0.1226	0.1394	0.1358	0.1442
120	0.2532	0.2680	0.2489	0.2752	0.2459	0.2870	0.2430	0.2326	0.2377	0.2326	0.2330
125	0.4144		0.3984		0.3888		0.3791		0.3602		0.3421
130	0.6108	0.6432	0.5769	0.6682	0.5582	0.6075	0.5396	0.5289	0.5032	0.4967	0.4681
135	0.8348		0.7781		0.7484		0.7190		0.6618		0.6068
140	1.0770	1.1042	0.9941	0.9005	0.9518	0.8433	0.9104	0.8433	0.8300	0.8398	0.7532
145	1.3280	1.3150	1.2160		1.1600		1.1060		1.0010	0.9648	0.9016
150	1.5750		1.4340		1.3650		1.2980		1.1690		1.0460
155	1.8080		1.6380		1.5570		1.4780		1.3250		1.1810
160	2.0150		1.8200		1.7270		1.6370		1.4640		1.3000
165	2.1880		1.9720		1.8690		1.7690		1.5780		1.3980
170	2.3180		2.0850		1.9750		1.8680		1.6640		1.4720
175	2.3980		2.1550		2.0400		1.9300		1.7170		1.5170
180	2.4250		2.1790		2.0620		1.9500		1.7350		1.5320

$$R(E_i) = \begin{cases} 0 & \text{for } E_i \leq I, \\ R_p & \text{for } E_i = E_p \\ R_F & \text{for } E_i \geq E_F > E_p. \end{cases} \quad (47)$$

First of the above three expressions in (47) suggests that no ionization takes place below the ionization threshold, the ionization potential of the atom. Here $R_p \approx 0.5$ is the value of R at $E_i = E_p$ with E_p being the incident energy at which the maximum absorption occurs. At impact energies $E_i \geq E_F$, well above the peak position E_p , the value of R increases to R_F (very close to 1). In the present study, we obtained $R_F \approx 0.8$ at 400 eV. The optimum values of the parameters A , B , and C are found to be -0.92 , -10.04 and 8.23 respectively.

2.4. NSA model for spin-zero nuclei

At very high energies, the influence of the target electrons is negligibly small. Hence, the static potential reduces to the nuclear potential which is generated from the nuclear ground-state charge distribution.

In our NSA calculations, we have modeled $\varrho_n(r)$ in two different ways. For one, we have used the analytical Fermi distribution

$$\varrho_{n1}(r) = \varrho_0 / (1 + \exp((r - c)/a)), \quad (48)$$

with the nuclear size parameter $c = 2.74$ fm and the surface diffuseness parameter $a = 0.572$ fm for the ^{20}Ne nucleus.⁵⁹⁾ ϱ_0 is the normalization constant according to (7).

Secondly, we have generated $\varrho_n(r)$ from the experimentally determined charge form factor $F_c(q)$, where q is the momentum transfer to the nucleus.¹⁹⁾ The conversion of $F_c(q)$ to $\varrho_n(r)$ is given by the inverse Fourier–Bessel transform³⁸⁾

$$\varrho_{n2}(r) = \frac{Z}{2\pi^2} \int_0^\infty q^2 dq F_c(q) j_0(qr), \quad (49)$$

where $j_0(x) = (\sin x)/x$ is a spherical Bessel function.

Apart from the differential cross section for potential scattering, as given by (32) in terms of the amplitudes $f(\theta)$ and $g(\theta)$, we also calculate the Sherman function, $S(\theta)$ using

Table IV. DCS (a_0^2/Sr) for the same as in Table I at energies 100, 150, 200, 300, 400 and 500 eV, Experimental reference(s): DuBois and Rudd¹⁵⁾ and Gupta and Rees.¹⁶⁾

θ	100 eV		150 eV		200 eV		300 eV		400 eV		500 eV	
	OPM	Exp. ¹⁵⁾	OPM	Exp. ¹⁶⁾	OPM	Exp. ¹⁵⁾	OPM	Exp. ¹⁶⁾	OPM	Exp. ¹⁶⁾	OPM	Exp. ¹⁵⁾
0	10.1500		11.1200		11.5000		11.8000		11.8900		11.9300	
2	9.4550		10.1800		10.3800		10.3900		10.2400		10.0900	
4	8.6430		9.1740		9.2310	10.4000	9.0510		8.7880		8.5450	9.0600
6	7.8900	7.1600	8.2560		8.2070	9.0200	7.8960		7.5540		7.2540	7.0800
8	7.1850	6.3400	7.4070		7.2710	7.8400	6.8540		6.4490		6.1030	5.5400
10	6.5220	5.5200	6.6140	7.110	6.4010	6.3000	5.8960	5.650	5.4420	5.390	5.0620	4.2400
12	5.8960	5.0400	5.8700		5.5910	5.4600	5.0160		4.5290		4.1320	3.5000
15	5.0250	4.3200	4.8440	4.750	4.4880	4.4000	3.8490	3.400	3.3500	3.110	2.9630	2.5800
20	3.7520	3.2500	3.3850	3.320	2.9680	3.0600	2.3390	2.080	1.9140	1.960	1.6160	1.5400
25	2.7160	2.3300	2.2590	2.220	1.8630	2.0400	1.3520	1.260	1.0580	1.150	0.8724	0.9110
30	1.9170	1.7100	1.4560	1.540	1.1310	1.3400	0.7743	0.865	0.6001	0.729	0.4996	0.5680
35	1.3350		0.9237	1.070	0.6852	0.8930	0.4637	0.559	0.3700	0.479	0.3166	
40	0.9317	0.9340	0.5943	0.771	0.4329	0.6190	0.3049	0.386	0.2536	0.340	0.2205	0.2680
45	0.6650		0.4011	0.525	0.2967		0.2227	0.304	0.1893	0.243	0.1638	
50	0.4926	0.5280	0.2906	0.382	0.2230	0.3010	0.1757	0.229	0.1492	0.169	0.1276	0.1470
55	0.3796		0.2255		0.1794		0.1447		0.1221		0.1037	
60	0.3009	0.3180	0.1825	0.183	0.1493	0.1770	0.1221	0.138	0.1032	0.103	0.0872	0.0967
65	0.2397		0.1497		0.1257		0.1055		0.0898		0.0752	
70	0.1871	0.1920	0.1218	0.094	0.1065	0.1140	0.0935	0.102	0.0800	0.082	0.0661	0.0715
75	0.1392		0.0978		0.0919		0.0852		0.0725		0.0590	
80	0.0961	0.1040	0.0788	0.076	0.0823	0.0892	0.0798	0.084	0.0668	0.067	0.0536	0.0556
85	0.0601		0.0660		0.0777		0.0766		0.0626		0.0494	
90	0.0341	0.0508	0.0606	0.075	0.0779	0.0820	0.0751	0.071	0.0597	0.057	0.0461	0.0479
95	0.0214	0.0432	0.0634		0.0824		0.0752		0.0578		0.0437	
100	0.0250	0.0499	0.0747	0.089	0.0907	0.0875	0.0766	0.070	0.0568	0.051	0.0417	0.0424
105	0.0469		0.0942		0.1025		0.0791		0.0563		0.0401	
110	0.0882	0.1140	0.1215	0.133	0.1172	0.1090	0.0825	0.071	0.0561	0.050	0.0388	0.0396
115	0.1491		0.1561		0.1345		0.0866		0.0563		0.0379	
120	0.2286	0.2530	0.1969	0.201	0.1541	0.1390	0.0911	0.078	0.0565	0.048	0.0371	0.0388
125	0.3247		0.2430		0.1753		0.0957		0.0569		0.0365	
130	0.4346	0.4730	0.2931	0.278	0.1977	0.1810	0.1004	0.087	0.0573	0.047	0.0360	0.0376
135	0.5546		0.3458		0.2207		0.1050		0.0578		0.0357	
140	0.6805	0.7330	0.3994	0.370	0.2436	0.2240	0.1094	0.111	0.0583	0.047	0.0354	0.0376
145	0.8075		0.4523		0.2658		0.1135		0.0588		0.0351	
150	0.9307	1.0300	0.5026	0.412	0.2867	0.2620	0.1172	0.153	0.0592	0.046	0.0350	0.0381
155	1.0450		0.5487		0.3055		0.1205		0.0596		0.0348	
160	1.1460		0.5890		0.3218		0.1232		0.0599		0.0347	
165	1.2300		0.6220		0.3350		0.1254		0.0602		0.0346	
170	1.2920		0.6464		0.3447		0.1270		0.0604		0.0345	
175	1.3300		0.6615		0.3507		0.1280		0.0605		0.0345	
180	1.3430		0.6666		0.3527		0.1283		0.0606		0.0345	

Eq. (33). This function describes the relative change of intensity when the spin of the projectile, oriented perpendicular to the scattering plane, is flipped. For high energies in the MeV region, the sum over phase shifts inherent in $f(\theta)$ and $g(\theta)$ is evaluated by means of a threefold convergence acceleration.⁶⁰⁾

3. Results and discussions

In this work, the ELSEPA code¹⁾ is used to calculate the scattering cross sections of electrons and positrons by the neutral atom and ions of neon. The DCSs for electron scattering calculated over a wide range of energy (3.4 eV–10 keV) are compared with the experimental data^{10,12,13,15,17)} and the theoretical calculations.^{32,33,35)} The DCSs for positron scattering are compared with the experimental data¹⁸⁾ and theoretical calculations.^{34,36,61)}

3.1. e^+ scattering by neutral neon

In Tables I–VI, We tabulate our predicted DCSs, obtained from OPM, for e^- -Ne scattering along with the experimental data.^{10–17)} We also provide graphical illustration for some of

these DCSs and compare with the available experimental measurements^{11–17)} and other theoretical calculations.^{32–35)}

At energy 3.4 and 4.2 eV, our calculations show significant differences with the experimental data.¹⁰⁾ Larger discrepancies are observed at small and higher angles. At energy 3.4 eV, maximum discrepancy of $\sim 60\%$ is observed at 15° , while at energy 4.2 eV, the same is $\sim 43\%$ at 130° . At energies 5.0, 7.0 and 7.5 eV, our calculations show more or less good agreements with the experimental data^{10,11)} except at higher angles. Besides the tabulated data, we present our DCS calculations for the impact energy 10 eV in Fig. 1(a) and we find a quite good agreement both qualitatively and quantitatively with the experimental data¹¹⁾ and the calculations of McEachran and Stauffer.³²⁾ However these two calculations disagree with those of Fon and Berrington.³³⁾

In Table II, we present our calculated DCS data along with the experimental data^{11–13)} at 12.5, 15, 17.5, 20, 30 and 40 eV. We find very a close agreement with the experimental data. Maximum 10% discrepancies are observed in these

Table V. DCS (a_0^2/Sr) for the same as in Table I at energies 600, 700, 750, 800, 900 and 1000 eV, Experimental reference(s): Bromberg,¹⁴⁾ DuBois and Rudd¹⁵⁾ and Jansen et al.¹⁷⁾

θ	600 eV	700 eV		750 eV		800 eV		900 eV	1000 eV	
	OPM	OPM	Exp. ¹⁴⁾	OPM	Exp. ¹⁷⁾	OPM	Exp. ¹⁵⁾	OPM	OPM	Exp. ¹⁷⁾
0	11.9800	12.0400		12.0800		12.1100		12.1700	12.2300	
2	9.9660	9.8770		9.8390		9.8040		9.7390	9.6790	
4	8.3500	8.2000		8.1350		8.0750	6.7200	7.9670	7.8690	
6	7.0110	6.8190		6.7350		6.6560	5.3400	6.5110	6.3800	
8	5.8220	5.5930	5.511	5.4910		5.3960	4.2400	5.2200	5.0590	
10	4.7530	4.5000	4.378	4.3870	3.9600	4.2810	3.4000	4.0870	3.9100	3.4800
12	3.8120	3.5510		3.4360		3.3290	2.6500	3.1340	2.9590	
15	2.6610	2.4200		2.3160	2.1700	2.2210		2.0510	1.9040	1.7800
20	1.3990	1.2370	1.285	1.1700	1.1900	1.1100	1.0000	1.0060	0.9194	0.9080
25	0.7472	0.6574	0.720	0.6208	0.6700	0.5883	0.5470	0.5323	0.4852	0.4980
30	0.4337	0.3852		0.3648	0.4010	0.3462	0.3320	0.3131	0.2843	0.2930
35	0.2790	0.2486		0.2351	0.2560	0.2226	0.2170	0.2000	0.1803	0.1880
40	0.1942	0.1719		0.1619	0.1740	0.1528	0.1530	0.1365	0.1226	0.1280
45	0.1429	0.1256		0.1181	0.1280	0.1112		0.0991	0.0889	0.0906
50	0.1104	0.0966		0.0907	0.0978	0.0852	0.0847	0.0756	0.0673	0.0683
55	0.0890	0.0774		0.0723		0.0677		0.0595	0.0524	
60	0.0741	0.0636		0.0591		0.0550	0.0546	0.0478	0.0418	
65	0.0630	0.0534		0.0493		0.0456		0.0393	0.0341	
70	0.0545	0.0456		0.0419		0.0386	0.0375	0.0329	0.0283	
75	0.0480	0.0396		0.0362		0.0332		0.0280	0.0239	
80	0.0429	0.0350		0.0318		0.0289	0.0282	0.0242	0.0205	
85	0.0389	0.0313		0.0282		0.0256		0.0213	0.0179	
90	0.0357	0.0283		0.0254		0.0229	0.0226	0.0189	0.0158	
95	0.0331	0.0259		0.0231		0.0208		0.0170	0.0141	
100	0.0310	0.0240		0.0213		0.0190	0.0189	0.0155	0.0128	
105	0.0293	0.0224		0.0198		0.0176		0.0142	0.0116	
110	0.0280	0.0211		0.0186		0.0164	0.0164	0.0131	0.0107	
115	0.0268	0.0200		0.0175		0.0155		0.0123	0.0100	
120	0.0259	0.0191		0.0167		0.0146	0.0146	0.0116	0.0094	
125	0.0252	0.0184		0.0159		0.0140		0.0110	0.0088	
130	0.0245	0.0177		0.0153		0.0134	0.0135	0.0105	0.0084	
135	0.0240	0.0172		0.0148		0.0129		0.0101	0.0080	
140	0.0235	0.0167		0.0144		0.0125	0.0132	0.0097	0.0077	
145	0.0231	0.0164		0.0140		0.0122		0.0094	0.0075	
150	0.0228	0.0161		0.0138		0.0119	0.0129	0.0092	0.0073	
155	0.0226	0.0158		0.0135		0.0117		0.0090	0.0071	
160	0.0224	0.0156		0.0134		0.0115		0.0088	0.0070	
165	0.0222	0.0155		0.0132		0.0114		0.0087	0.0069	
170	0.0221	0.0154		0.0131		0.0113		0.0086	0.0068	
175	0.0220	0.0153		0.0131		0.0113		0.0086	0.0068	
180	0.0220	0.0153		0.0131		0.0112		0.0086	0.0068	

energies. Our method produces minima in DCSs almost accurately. At 20 eV, our calculated minimum coincides with the experimental minimum at 115°. At 30 eV, present method predicts a minimum at 110°, while the experimental one is observed at 115°. At 40 eV, experimental minimum is at 110° and our method predicts that minimum at 105°. DCSs at 15, 20, 30 and 40 eV are graphically illustrated in Figs. 1(b)–1(e) along with the experimental^{11–13,15)} and theoretical data.^{32,33)} Our calculations and those of McEacharan and Stauffer³²⁾ and Fon and Berrington³³⁾ agree closely with the experimental observations.^{11–13,15)} Our predicted minima in DCSs are close to those provided by McEacharan and Stauffer³²⁾ (Fig. 1). The cross section values of these two calculations are also close to each other.

In Table III, we present our DCS results at 50, 60, 65, 70, 80 and 90 eV along with the experimental data.^{15,16)} As seen in the table, a close agreement between our result and data is produced. At 70 and 80 eV, our results underestimate the

minima in DCSs. In Tables IV, V and VI, we tabulate our calculations and compare with available experimental data.^{15–17)} We see very close agreement of our DCS results with the experimental data except for minor underestimation of cross section at the minimum point for 100 eV. Beyond 200 eV no minimum or maximum is observed, signifying that no interference of waves emitted from bound electrons occur. To the best of our knowledge, at 600, 900 eV and 5000–10000 eV, neither experimental data nor calculations are found for comparison. Some of these DCSs are graphically presented in Figs. 2 and 3 along with other theoretical calculations^{33–35)} and compared with the available experimental data.^{12–17)} R-matrix calculations³³⁾ show a slight shift of minima in DCSs to the right. Calculations of Byron et al.³⁴⁾ underestimate the DCSs values at higher angles at energies 100, 200 and 300 eV.

In Figs. 4(a)–4(f), we present DCSs for elastic scattering of positron from Neon. At energy 13.6 eV DCSs of our

Table VI. DCS (a_0^2/Sr) for the same as in Table I at energies 2000, 3000, 4000, 5000, 6000, 7000, 8000, 9000 and 10 000 eV. The actual DCS values multiplied by 10^3 is presented in this table. Experimental reference(s): Jansen et al.¹⁷⁾

θ	2000 eV		3000 eV		4000 eV	5000 eV	6000 eV	7000 eV	8000 eV	9000 eV	10000 eV
	OPM	Exp. ¹⁷⁾	OPM	Exp. ¹⁷⁾	OPM	OPM	OPM	OPM	OPM	OPM	OPM
0	12 540		12 630		12 662	12 669	12 670	12 669	12 669	12 671	12 675
2	9224.0		8901.0		8651.0	8443.0	8260.0	8093.0	7937.0	7788.0	7645.0
4	7157.0		6617.0		6143.0	5713.0	5321.0	4963.0	4637.0	4340.0	4069.0
6	5373.0		4604.0		3975.0	3457.0	3028.0	2671.0	2371.0	2117.0	1901.0
8	3852.0		3027.0		2431.0	1989.0	1654.0	1395.0	1191.0	1028.0	895.10
10	2675.0	2410	1943.0	1840	1470.0	1148.0	918.50	750.20	623.10	525.00	447.80
12	1834.0		1251.0		904.90	682.20	530.70	423.40	344.90	286.00	240.80
15	1053.0	992	672.50	662	463.00	335.80	253.70	198.10	158.90	130.30	108.70
20	460.30	442	272.50	277	178.10	125.30	92.860	71.470	56.660	46.030	38.160
25	228.20	223	129.50	135	83.090	57.470	42.020	32.090	25.330	20.510	16.960
30	127.00	127	70.660	72.7	44.310	30.290	22.020	16.720	13.140	10.610	8.7610
35	78.210	78.4	42.150	43.3	26.080	17.660	12.740	9.6470	7.5600	6.0880	5.0170
40	51.360	51.3	27.000	27.6	16.470	11.070	7.9570	5.9950	4.6910	3.7710	3.0980
45	35.410	35.4	18.240	18.4	11.000	7.3480	5.2570	3.9540	3.0820	2.4740	2.0300
50	25.480	25.3	12.840	13.2	7.6820	5.1030	3.6390	2.7280	2.1240	1.7000	1.3940
55	18.920		9.3830		5.5630	3.6810	2.6170	1.9560	1.5200	1.2150	0.9935
60	14.440		7.0590		4.1620	2.7400	1.9420	1.4500	1.1230	0.8968	0.7319
65	11.310		5.4560		3.1950	2.0980	1.4820	1.1030	0.8541	0.6800	0.5549
70	9.0570		4.3200		2.5150	1.6440	1.1580	0.8611	0.6645	0.5287	0.4306
75	7.3930		3.4880		2.0200	1.3160	0.9253	0.6855	0.5285	0.4199	0.3414
80	6.1460		2.8710		1.6540	1.0730	0.7524	0.5568	0.4284	0.3397	0.2761
85	5.1960		2.4040		1.3780	0.8912	0.6229	0.4595	0.3531	0.2798	0.2270
90	4.4580		2.0420		1.1640	0.7503	0.5232	0.3856	0.2958	0.2339	0.1897
95	3.8770		1.7600		0.9985	0.6413	0.4459	0.3278	0.2511	0.1985	0.1608
100	3.4150		1.5370		0.8673	0.5550	0.3851	0.2827	0.2162	0.1706	0.1381
105	3.0420		1.3570		0.7620	0.4860	0.3364	0.2465	0.1884	0.1486	0.1202
110	2.7390		1.2120		0.6773	0.4307	0.2975	0.2176	0.1660	0.1308	0.1057
115	2.4920		1.0940		0.6083	0.3855	0.2657	0.1941	0.1480	0.1165	0.0941
120	2.2880		0.9963		0.5515	0.3485	0.2397	0.1749	0.1332	0.1048	0.0846
125	2.1180		0.9158		0.5047	0.3182	0.2185	0.1592	0.1212	0.0953	0.0769
130	1.9770		0.8490		0.4662	0.2931	0.2009	0.1463	0.1112	0.0874	0.0705
135	1.8600		0.7935		0.4342	0.2723	0.1864	0.1356	0.1030	0.0809	0.0652
140	1.7620		0.7476		0.4078	0.2551	0.1744	0.1268	0.0963	0.0756	0.0609
145	1.6820		0.7097		0.3859	0.2411	0.1647	0.1196	0.0908	0.0713	0.0574
150	1.6160		0.6787		0.3681	0.2296	0.1567	0.1137	0.0863	0.0677	0.0545
155	1.5630		0.6538		0.3538	0.2205	0.1502	0.1090	0.0826	0.0648	0.0522
160	1.5210		0.6341		0.3426	0.2132	0.1452	0.1053	0.0798	0.0626	0.0504
165	1.4890		0.6193		0.3342	0.2078	0.1414	0.1025	0.0777	0.0609	0.0490
170	1.4670		0.6089		0.3284	0.2039	0.1387	0.1006	0.0762	0.0598	0.0481
175	1.4540		0.6028		0.3249	0.2017	0.1372	0.0995	0.0754	0.0591	0.0476
180	1.4500		0.6008		0.3237	0.2010	0.1367	0.0991	0.0751	0.0589	0.0474

calculations and that of Gianturco et al.⁶¹⁾ are in good agreement with the experimental data.¹⁸⁾ At 20 eV, our DCS results show good agreement except at the minimum region, showing better agreement than those of Baluja et al.³⁶⁾ and Stepanek.⁶²⁾ Calculations of Stepanek⁶²⁾ overestimate the experimental values and show significant difference with the calculations of ours and Baluja et al.³⁶⁾ At 50 eV, predictions by Baluja et al.³⁶⁾ is better than our calculations with noticeable discrepancies at lower and higher scattering angles. At 200 eV, our calculations show good agreement with the experimental data¹⁸⁾ and the calculations of Byron et al.³⁴⁾ while predictions of Baluja et al.³⁶⁾ show significant discrepancies. At 100 eV, our calculations show close agreement with those of Baluja et al.³⁶⁾ except at the angular region $\sim 60^\circ - 120^\circ$. Calculations of Byron et al. and Stepanek⁶²⁾ poorly agree with above two results. At 300 eV, our calculations are

compared with those of Byron et al.³⁴⁾ Both the calculations more or less agree with one another except at the angular region $\sim 30^\circ - 60^\circ$.

In Fig. 5, we present the energy variation of the DCS and the Sherman function S for the elastic scattering of electrons at the scattering angles 50° , 90° and 130° . OPM is used from 1 eV–1 MeV, and the NSA method is applied from 1 keV to 0.5 GeV. The DCSs calculated from this combined methods show very close agreement with the available data^{10,12,17,19)} both at low and high energies. In the keV and MeV energy ranges, a monotonous behavior of the DCSs is predicted by both OPM and NSA methods. At very high energies, the DCS shows a diffraction pattern, since the electron comes so close to the nucleus that the protons act as distinct scattering centers which causes interference effects. Since minima in the cross section correspond to maxima in the spin asymmetry, the diffraction structures are also present in S . At

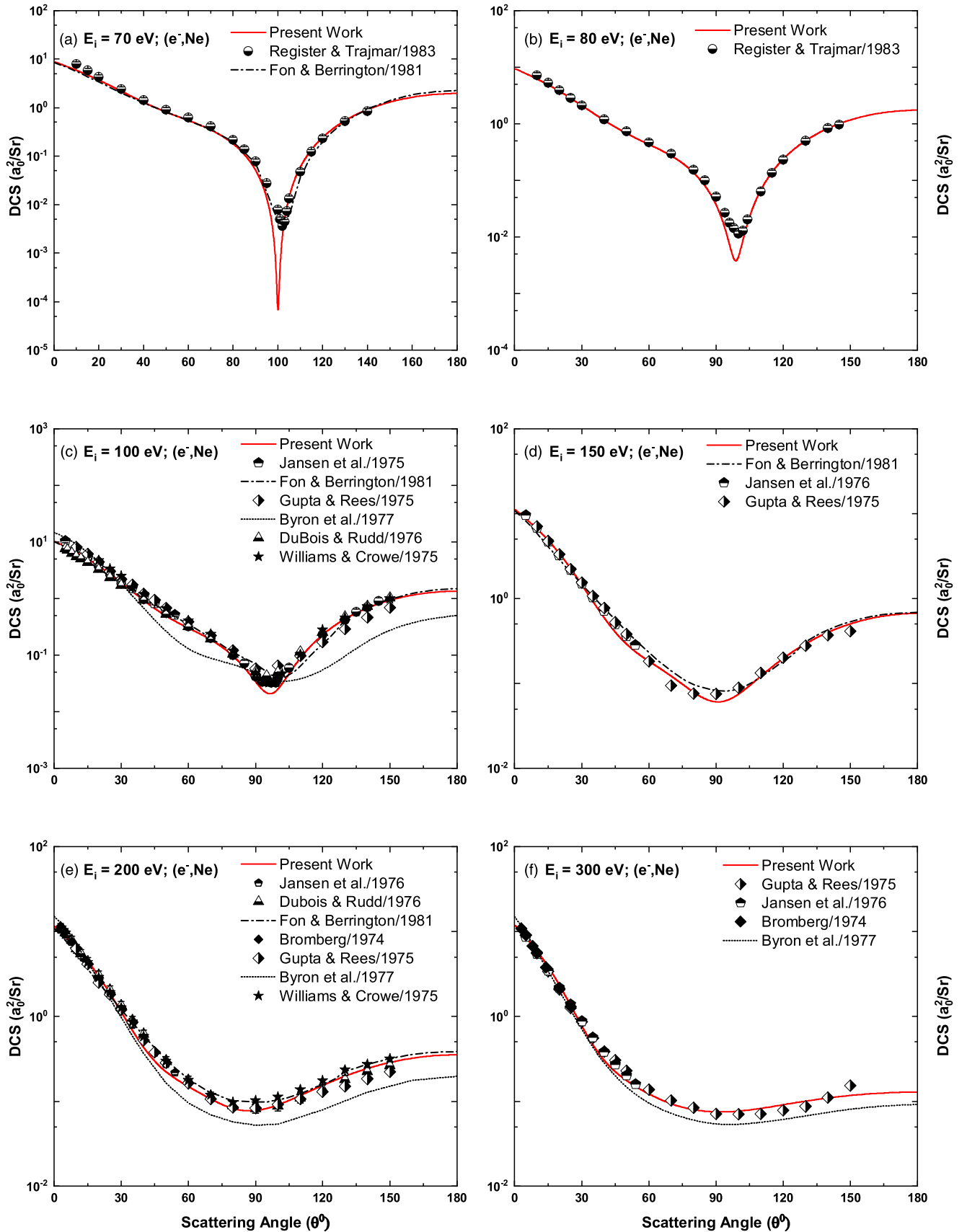


Fig. 2. (Color online) DCS (a_0^2/Sr) for the same as in Fig. 1 at energies 70, 80, 100, 150, 200 and 300 eV. Theoretical: Fon and Berrington³³⁾ and Byron et al.³⁴⁾ Experimental: Brewer et al.¹¹⁾ Register and Trajmar,¹²⁾ Jansen et al.¹⁷⁾ Gupta & Rees,¹⁶⁾ DuBois and Rudd¹⁵⁾ and Williams and Crowe.¹³⁾

lower energies there are oscillations, which decrease in amplitude with increase of angle. It is only in this regime, above 150 MeV for 130° , where the results from the two charge distributions $\varrho_{n1}(r)$ and $\varrho_{n2}(r)$, taken from (48) and

(49), are different, pointing to the sensitivity to nuclear structure effects.

In Fig. 6, we depict the energy variation of the DCSs and the Sherman function for positron scattering at 60° , 90° and

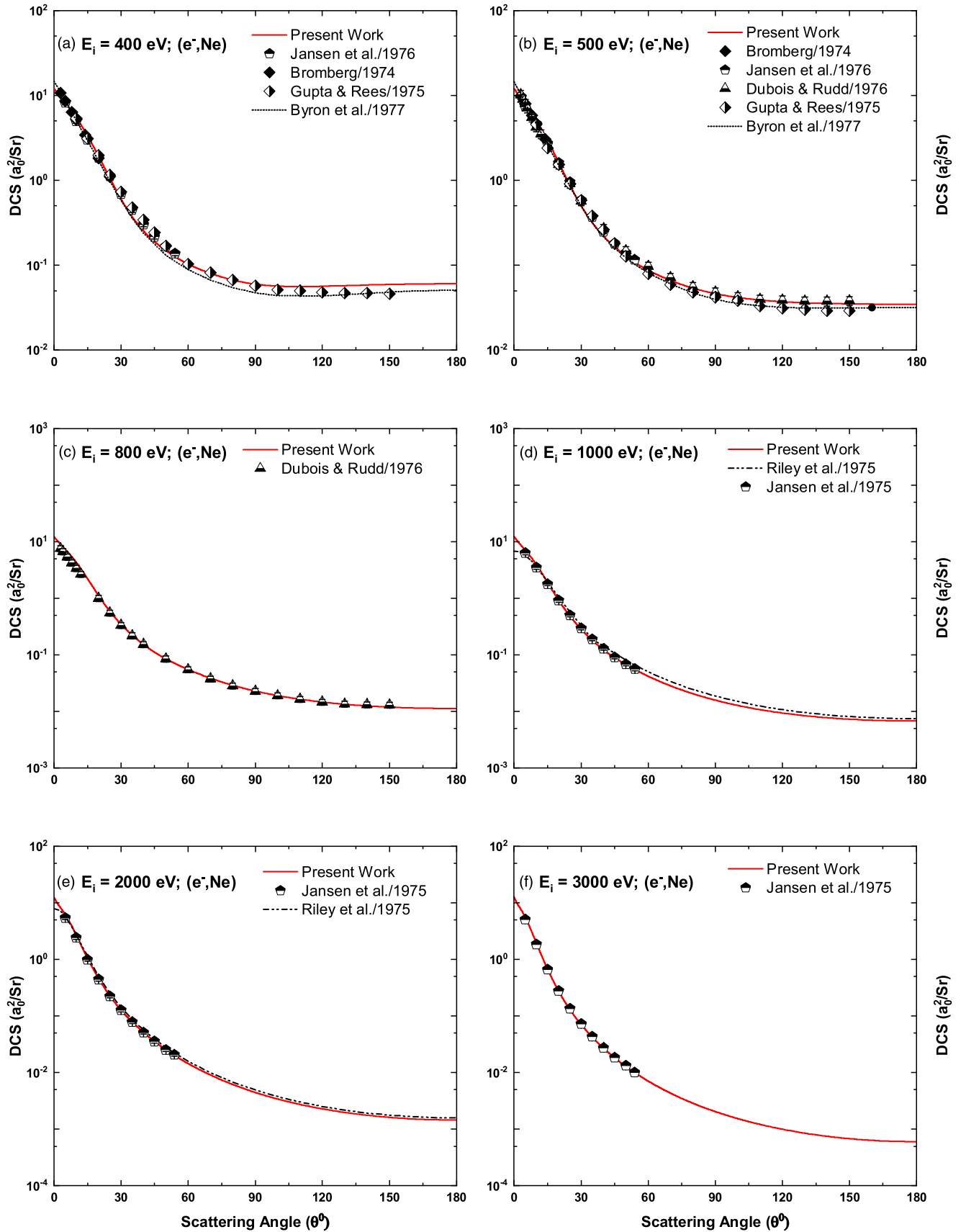


Fig. 3. (Color online) DCS (a_0^2/Sr) for the same as in Fig. 1 at energies 400, 500, 800, 1000, 2000 and 3000 eV. Theoretical: Byron et al.³⁴⁾ and Riley et al.³⁵⁾ Experimental: Jansen et al.¹⁷⁾ Gupta & Rees,¹⁶⁾ DuBois and Rudd¹⁵⁾ and Bromberg.¹⁴⁾

130°. Our calculated DCSs show reasonable agreement with the experimental data¹⁸⁾ at the scattering angles 60° and 90° and quite satisfactory agreement at 130°. A monotonous

behavior of the DCS in the keV and MeV energy range and an interference pattern in the GeV range is also observed for positron scattering. The extremely small values of S for

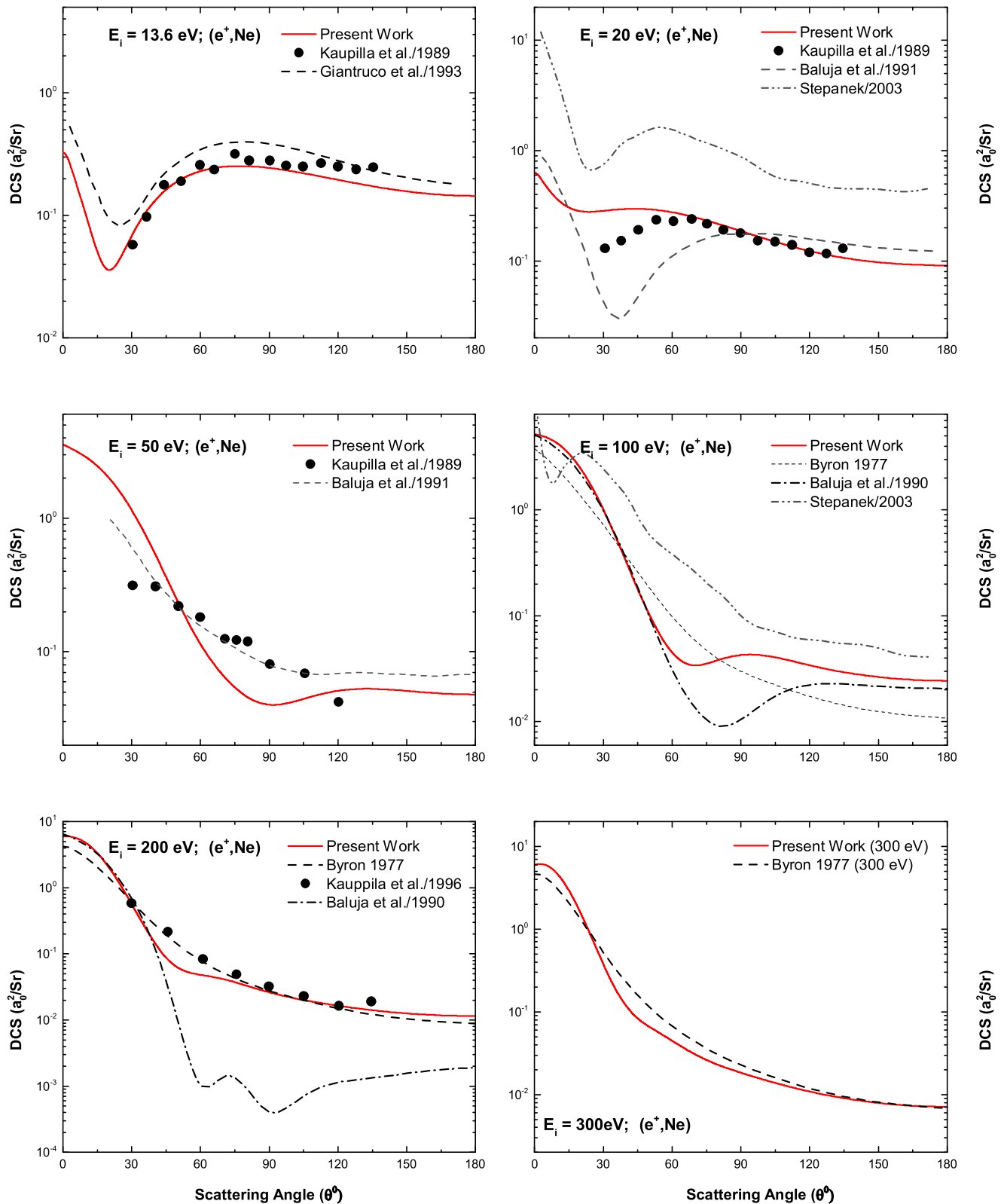


Fig. 4. (Color online) DCS (a_0^2/Sr) for the elastic $e^+-\text{Ne}$ scattering at energies 13.6, 20, 50, 100, 200 and 300 eV. Theoretical: Byron et al.³⁴⁾ Baluja et al.³⁶⁾ Gianturco et al.⁶¹⁾ and Stepanek.⁶²⁾ Experimental: Kaupilla et al.¹⁸⁾

positrons at energies below 1 keV are common to all targets, which is discussed in detail in.⁶³⁾

A comparison between the electron and positron energy dependence of Sherman function is illustrated in Fig. 7. It is observed that the strict antisymmetry between electron and positron spin polarizations, predicted with the help of second

order Born approximation, is broken by the distortion from electronic and nuclear potentials. The extremum of the Sherman function for positrons is shifted to higher energies as compared to that for electrons. Tolhoek predicted such a feature for $z = 80$ nucleus.⁶⁴⁾ This feature is also observed for medium-heavy and light nuclei.^{63,65)}

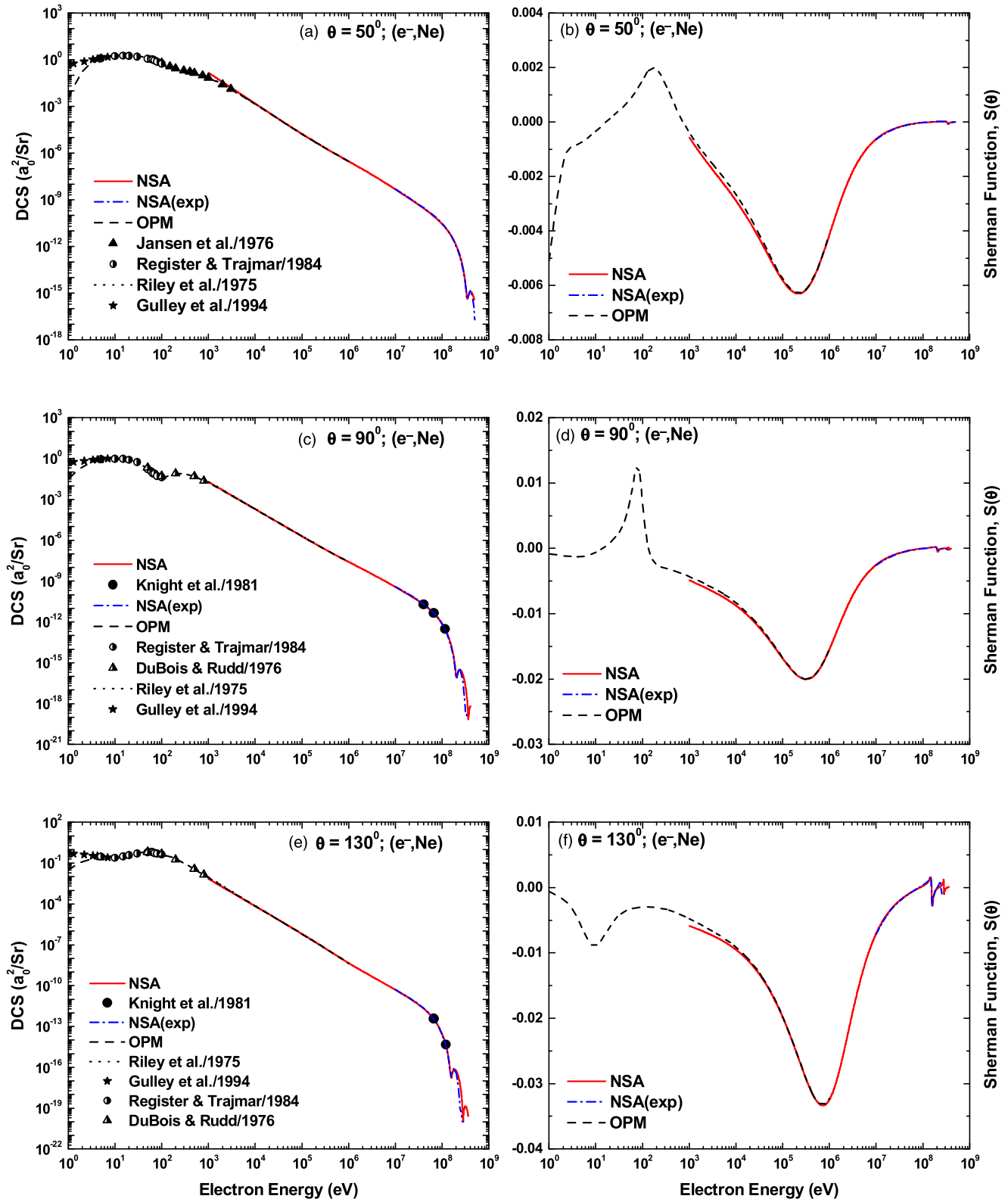


Fig. 5. (Color online) Energy variation of DCS (a_0^2/Sr) and Sherman for the e^- -Ne scattering at the scattering angles 50° , 90° and 130° . Shown are the OPM results (---, black) and the NSA results (—, red, using the Fermi distribution q_{n1} ; ---, using q_2 from the experimental form factor). Theoretical: Riley et al.³⁵ Experimental: Gulley et al.¹⁰ Register and Trajmar,¹² DuBois and Rudd¹⁵ and Jansen et al.¹⁷ The high-energy experimental data points are obtained by interpolating the tabulated results of Knight et al.¹⁹

In Figs. 8–10, we present our investigations of CM in DCSs of electron scattering by Ne. In Fig. 8(a), we show the variation of scattering angles of DCS minima with energy. We see the presence of lower angle minima in the energy range 15–20 eV and the intermediate angle minima in the

energy range 5–400 eV. It is apparent from Fig. 8(b) that, there is no CM in lower angle DCSs (curve 1), but a CM is present both in experimental data and theoretical calculations in the intermediate angle DCSs (curve 2). Our calculations of the DCS minima and their variation with energy predict a

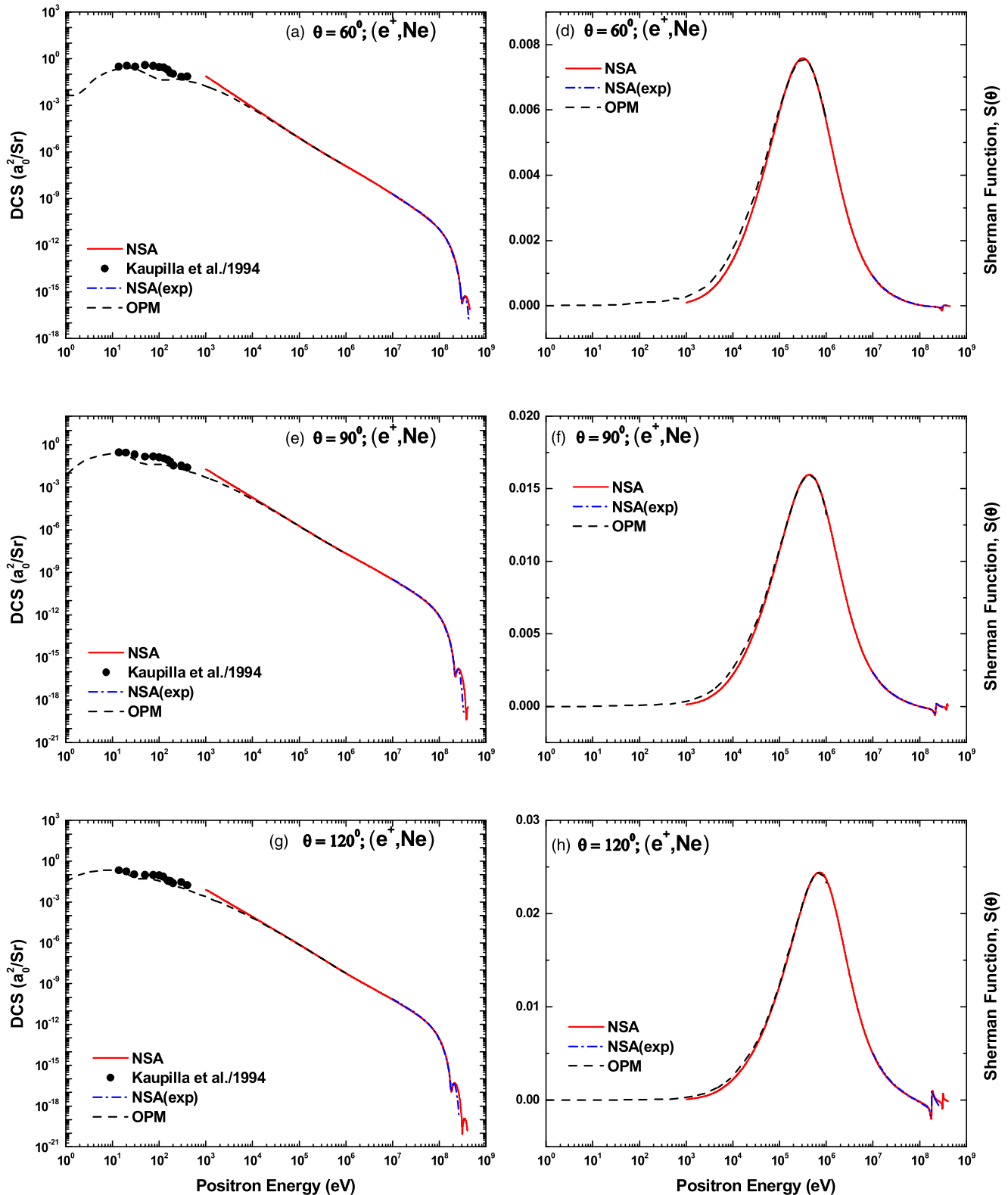


Fig. 6. (Color online) Same as in Fig. 8 but for positron impact at the scattering angles 60° , 90° and 120° . Shown are the OPM results (---, black) and the NSA results (—, red). Experimental: Kaupilla et al.¹⁸⁾

CM at energy 69.31 eV. Figure 8(c) also shows significant spin polarization at 69.31 eV. Figure 8(d) shows that the minima at 68.50 and at 70.50 eV are higher than the minimum at 69.31 eV and this minimum occurs at angle 100° . The above investigations predict that, there is only one CM and it is at $E_c = 69.31$ eV, $\theta_c = 100^\circ$. Three dimensional plot of DCS and Sherman function in Figs. 9 and 10 also predict only one CM in DCSs of elastic scattering of

electrons by Ne. In Table VII, we compare our prediction with experiments and theory.

Kollath et al.⁷⁾ and Register and Trajmar¹²⁾ experimentally found the CM at $E_c = 73.7$ eV, $\theta_c = 100^\circ$ and $E_c = 62.5$ eV, $\theta_c = 101.7^\circ$ respectively. Considering exchange and distortion and using partial wave technique Jhanwar et al.⁶⁶⁾ calculated CM at $E_c = 66.5$ eV, $\theta_c = 93.3^\circ$. Thompson⁶⁷⁾ and Walker⁸⁾ respectively using non-relativistic

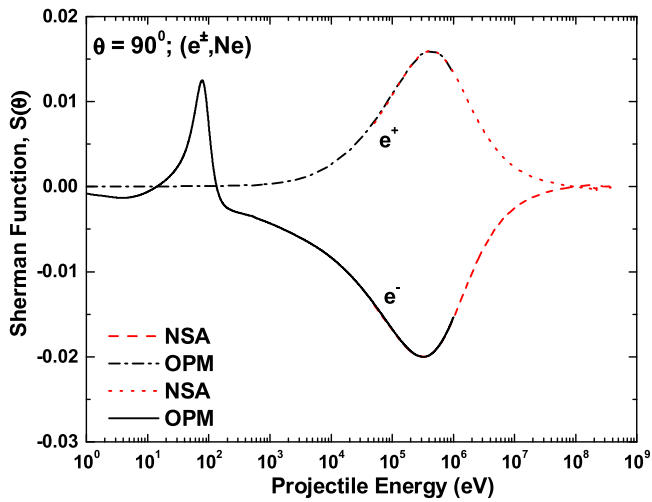


Fig. 7. (Color online) Comparison of Sherman function $S(\theta)$, in respective order, for electron and positron scattering from neon at the scattering angle 90° .

and relativistic calculations obtained almost the same results for CM (Table VII). Considering exchange, distortion and absorption McCarthy⁶⁸ used the optical model and predicted the CM at $E_c = 66.2$ eV, $\theta_c = 99.6^\circ$. Using the R-matrix calculations Blum and Burke⁶⁹ produced the CM at $E_c = 66.1$ eV $\theta_c = 102^\circ$.

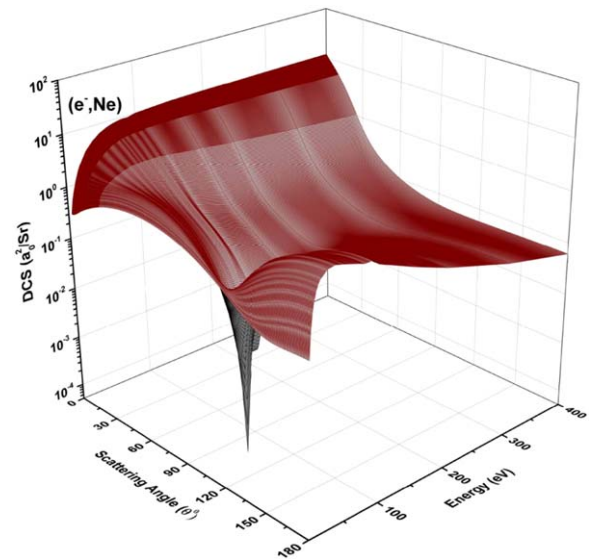


Fig. 9. (Color online) Energy dependence of angular distribution of DCS for electron-neon scattering depicting CM in DCSs.

In Fig. 11, we depict IECS, MTCS, VICS, INCS, TCS and TICS for elastic scattering of electron for Ne. In Fig. 11(a), OPM calculated IECSs show satisfactory agreement with the experimental measurements^{10,13,17,20} and theoretical calculations^{32,73} at energies above 7 eV, with noticeable

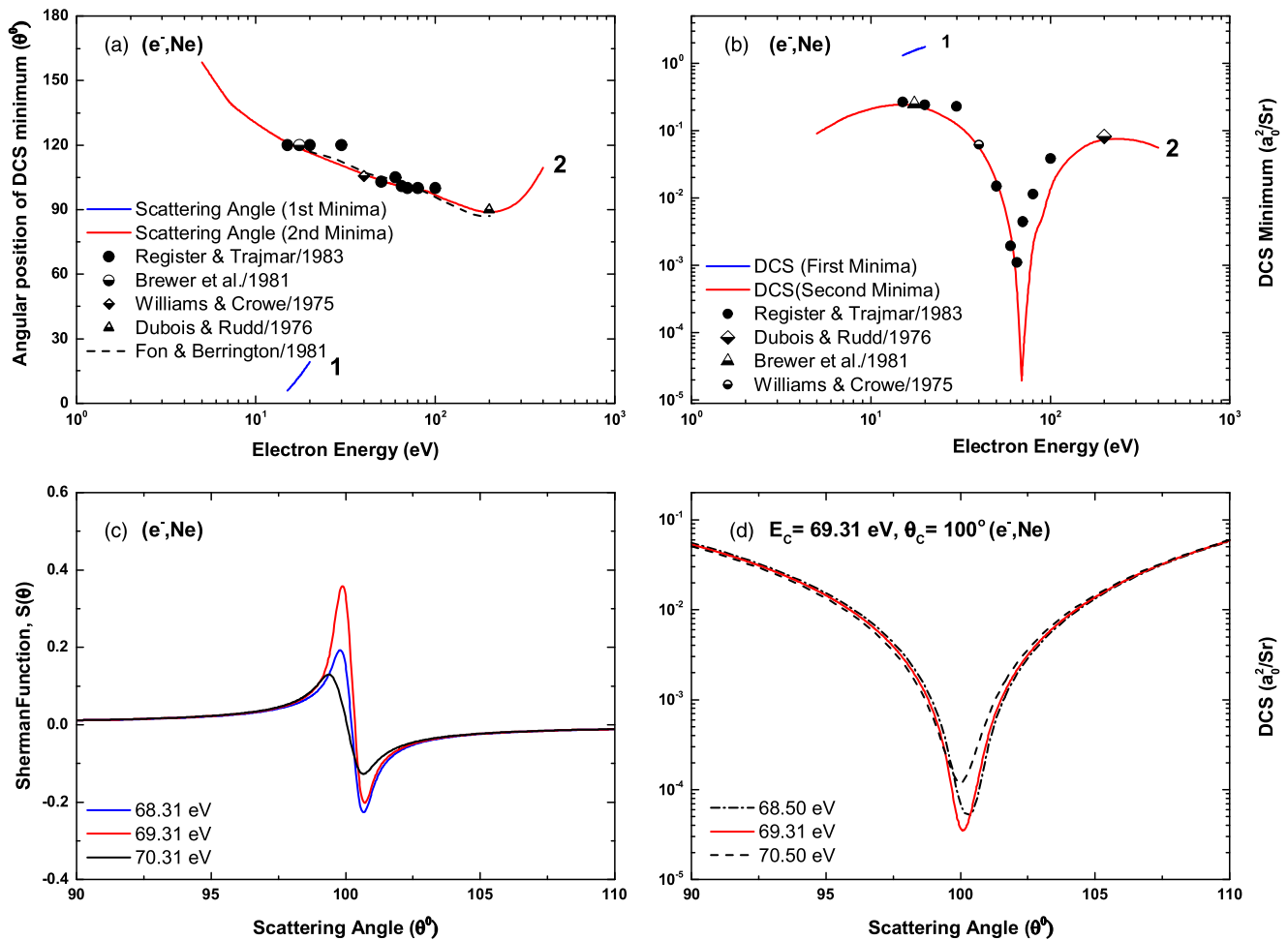
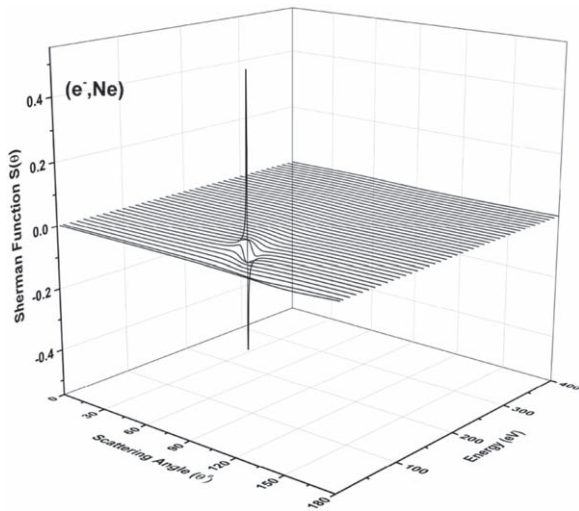


Fig. 8. (Color online) Energy dependence of the scattering angles of minimum DCS points (a) and that of minimum DCSs (b) for lower angle (curve 1) and intermediate angle (curve 2). Experimental: Brewer et al.¹¹ Williams and Crowe¹³ and DuBois and Rudd.¹⁵ Theoretical: Fon and Berrington.³³ Angular dependence of Sherman function at collision energies 68.31, 69.31 and 70.31 eV (c) and that of DCSs at incident energies 68.50, 69.31 and 70.50 eV (d).

Table VII. Critical minima (critical energy, E_c and angle, θ_c) positions for elastic e^- –Ne scattering.

Present work		Experimental		Theoretical	
E_c (eV)	θ_c	E_c (eV)	θ_c	E_c (eV)	θ_c
69.31	100.0°	73.7	100.0° ⁷⁾	66.5	093.3° ⁶⁶⁾
		62.5	101.7° ¹²⁾	60.2	102.8° ⁶⁷⁾
				60.6	102.6° ⁶⁸⁾
				66.2	099.6° ⁶⁸⁾
				66.1	102.0° ⁶⁹⁾

**Fig. 10.** Energy and angular dependence of Sherman function for electron-neon scattering.

discrepancies at lower energies. In Fig. 11(b), we present MTCSs and the agreement between theoretical calculations and experiment observations was fair beyond $E_i \approx 10$ eV. There is no experimental or theoretical data for VICs of elastic scattering of electron by Ne. We present the energy variation of VICs for prospective workers to compare with. Our INCS results are in good agreement with the semiempirical data of de Heer et al.²⁰⁾ barring low energies as evident from Fig. 11(d). TCS, shown in Fig. 11(e), produce close agreement with the experimental data^{22–26)} with noticeable discrepancies below the energy ~ 10 eV, while McEachran and Stauffer³²⁾ and Dewangan et al.⁷³⁾ closely reproduce the TCS data in their respective energy ranges. The OPM results might have been improved if we could use non-local optical potential. Our TICS calculations reproduce the one or another source of experimental data^{20,70–72)} well. Calculations of Bartlett and Stelbovics⁷⁴⁾ perform better than our calculations through the energy range.

In Fig. 12, we depict IECS, MTCS, VICs, INCS, TCS and TICS for elastic scattering of positron for Ne. In Fig. 12(a), we compare IECSs with the prediction of Dewangan and Walter⁷³⁾ and in Fig. 12(b), we compare MTCSs with the calculations McEachran et al.⁸⁰⁾ and we see fairly good agreement between the calculations in both cases. We present the predictions of VICs and INCS for future reference. We present our TCS results along with the experimental measurements.^{18,27–30)} There is quite satisfactory agreement between our calculations and experimental data. As evident

from Fig. 12(f), our TICS results are in fair agreement with the total ionization^{78,79)} and single ionization experimental data^{75–77)} and comparable with the theoretical predictions.^{81,82)}

3.2. e^- scattering by neon ions ($\text{Ne}^+ - \text{Ne}^{10+}$)

In Fig. 13, we present our DCSs results for the scattering of electron from $\text{Ne}^+ - \text{Ne}^{10+}$. It is observed that, DCS at a particular energy and angle increases with the increase of ionicity in conformity with the Rutherford scattering formula. It is also observed that increasing ionicity weakens the interference pattern. This is, perhaps, the contribution of the short range potential of the bound electrons decreases with the increase of charge state. In case of electron argon ion scattering, this observation is testified.^{83,84)} The sharp structure is observed in the angular distribution of the scattered electrons at low energies due to the interference between scattered waves due to the short range and Coulombic potentials. At low such energies, the short range potential becomes important due to the enhanced electron–electron correlations, as the velocity of the free electron becomes comparable to that of the dressing electrons of the ionic core.

In Figs. 14(a)–14(c), we present the IECSs for the scattering of electrons from different charge states. It is apparent from Fig. 14(a) that at lower degrees of ionicity, cross section increases with the increase of ionicity, albeit slightly. This is due to the diminution of the screening effect of the surrounding electron cloud. However at higher degrees of ionicity, the difference in cross sections is not appreciable at lower energies but show slight differences at higher energies. The screening effect is also seen at higher energies. Figures 14(d)–14(f) shows the energy variation of MTCSs for the ions of the neon isonuclear series. The dependence of the cross-section with the degree of ionicity follows the similar trend to that of IECS.

4. Conclusion

Within the framework of Dirac partial wave analysis, a complex e^\pm -atom potential, including static, exchange, correlation-polarization and absorption components, is employed to calculate DCS, IECS, MTCS, VICs, INCS, TCS and TICS. We present the DCSs for the scattering angles 0° – 180° for an energy range 3.4 eV–10 keV for electron scattering and 13.6–300 eV for positron scattering. We also depict the energy variation of DCS and Sherman function for e^\pm -Ne scattering for a wide energy range 1 eV–0.5 GeV. We present our calculations for IECS, MTCS, VICs, INCS and TCS for the energy range 1 eV–10 keV and TICS for the

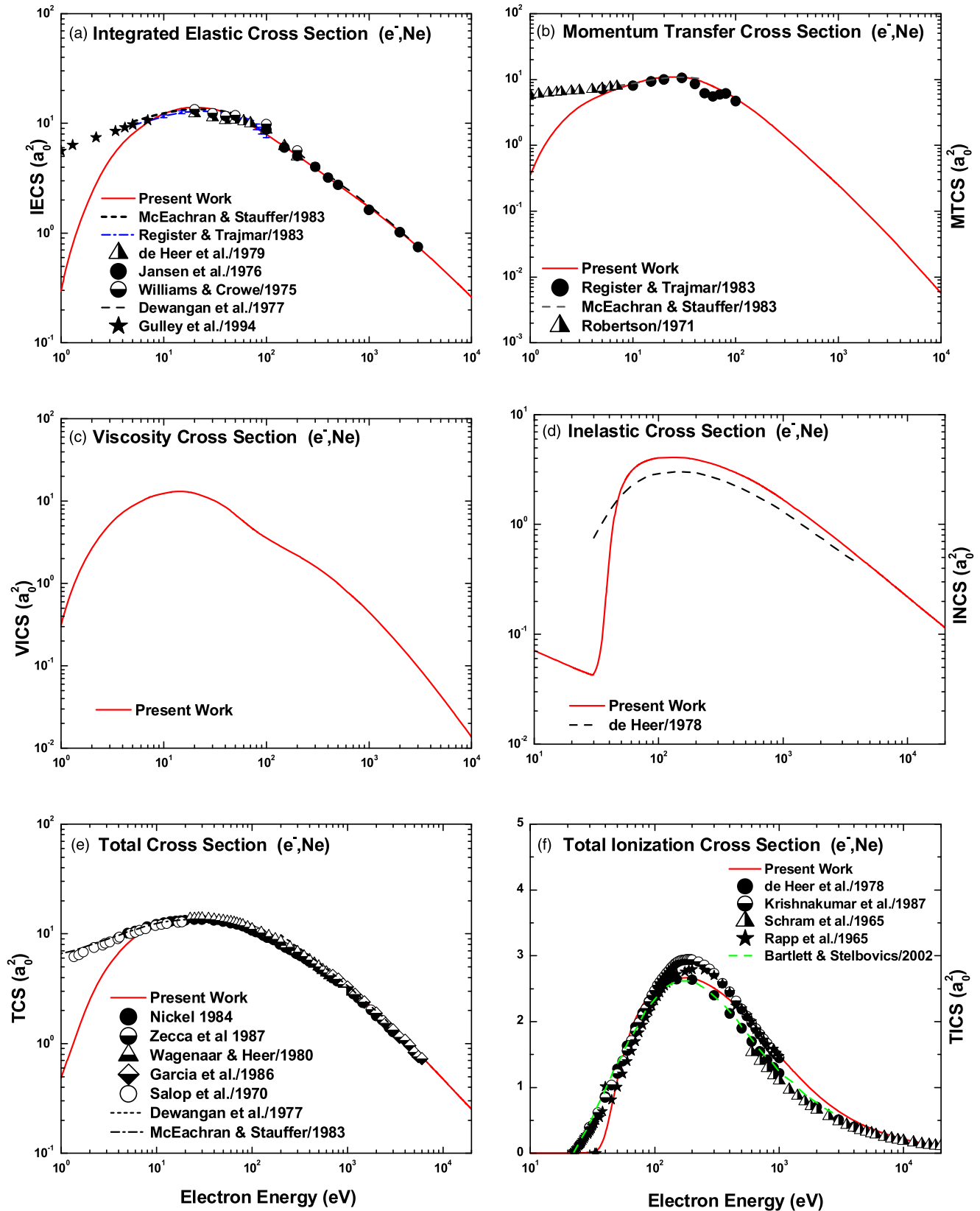


Fig. 11. (Color online) Energy dependence of (a) IECS, (b) MTCS, (c) VICS, (d) INCS and (e) TCS for e^- -Ne scattering. Experimental: (a), ^{13,17,20} (b), ^{12,21} (e) ^{22–26} and (f), ^{20,70–72} Theoretical: (a) and (b), ³² (e) ^{32,73} and (f), ⁷⁴ Semiempirical for (d), ²⁰

energy range 10 eV–20 keV. In case of electron scattering, our calculations show more or less good agreement at and beyond 10 eV, but produce poor agreement below 10 eV. This indicates that this method of calculations is not useful

for the scattering of electron and positron for low energy scattering. Effective range theory may be needed to complement this method. Our predicted minima in the DCSs of electron scattering in the range 15–300 eV are comparable to

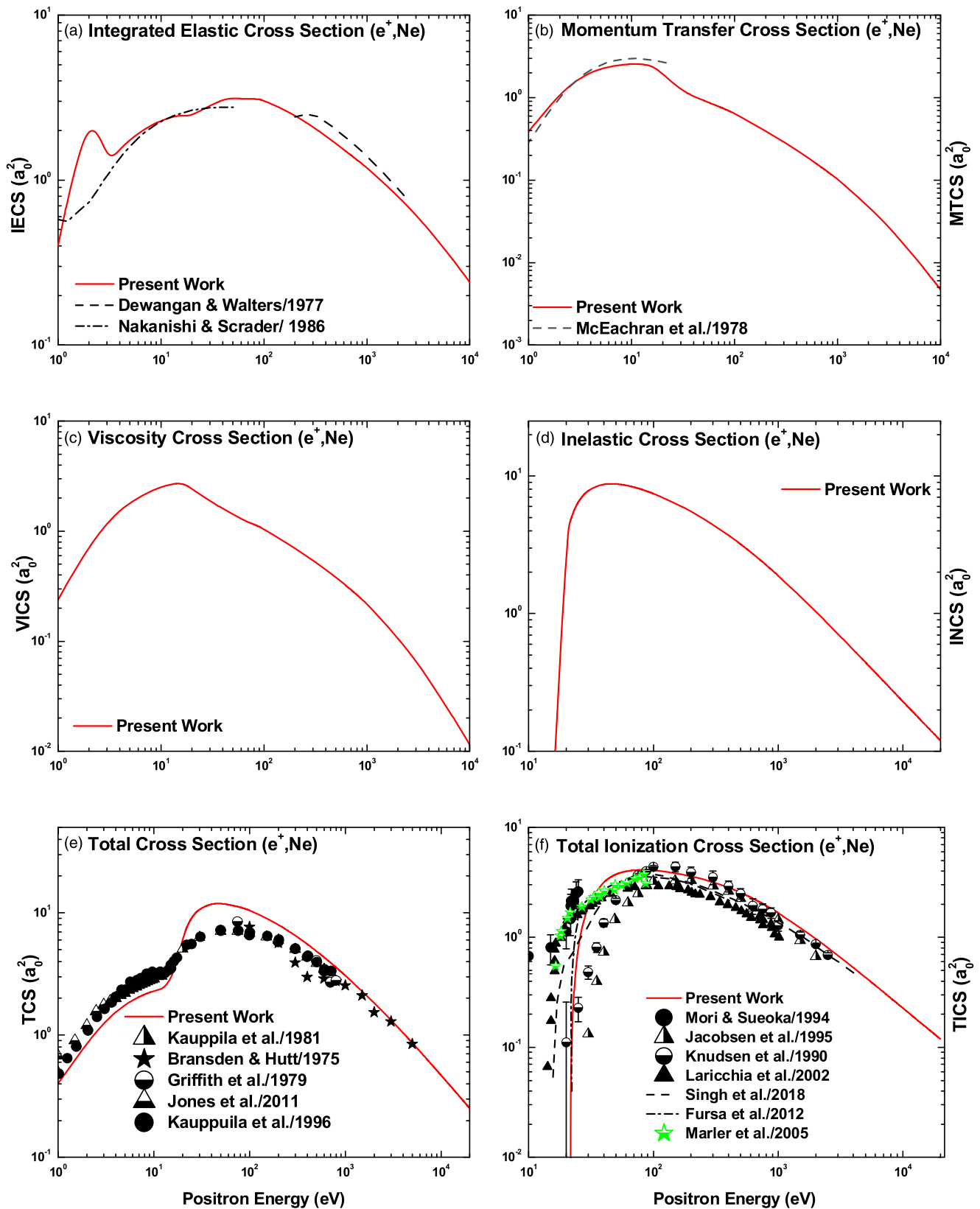


Fig. 12. (Color online) Energy dependence of (a) IECS, (b) MTCS, (c) VICS, (d) INCS and (e) TCS for e^+ -Ne scattering. Experimental: (e) ^{18,27–30} and (f) ^{75–79}. Theoretical: (a), ⁷³ (b) ⁸⁰ and (f) ^{81,82}.

other calculations. Our analysis of DCS and Sherman function reveals a CM at $E_c = 69.31$ eV, $\theta_c = 100^\circ$, fairly agreeing with experiments and other calculations. In literature, the experimental data for positron scattering is scant.

Our calculations show more or less good agreement with the available experimental data.

Performance level of our calculations at low energies is not satisfactory. This is due to the local approximation of

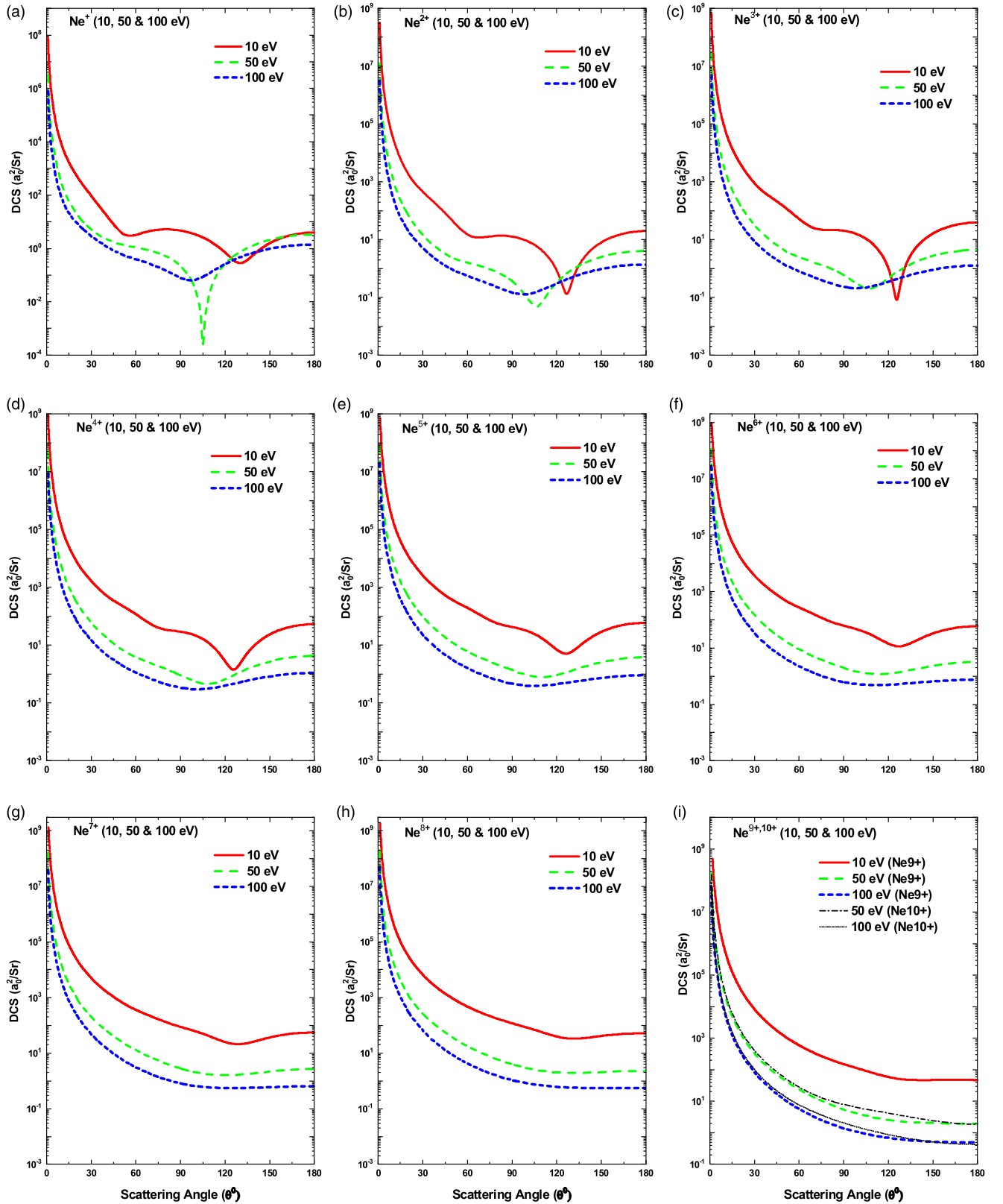


Fig. 13. (Color online) DCSs for the elastic scattering of electron from $\text{Ne}^+ - \text{Ne}^{10+}$.

the many-body non-local optical potential. Our results show a blending of good and poor agreements with those of Fon et al.³³⁾ Byron et al.³⁴⁾ and Riley et al.³⁵⁾ Satisfactory results obtained in this work are due to the choice of relativistic collision dynamics, accurate target

electron density and proper combinations of the optical potential components. This method adopted in this work can be easily implemented to generate reasonably accurate cross sections required for applications in science and industrial technologies.

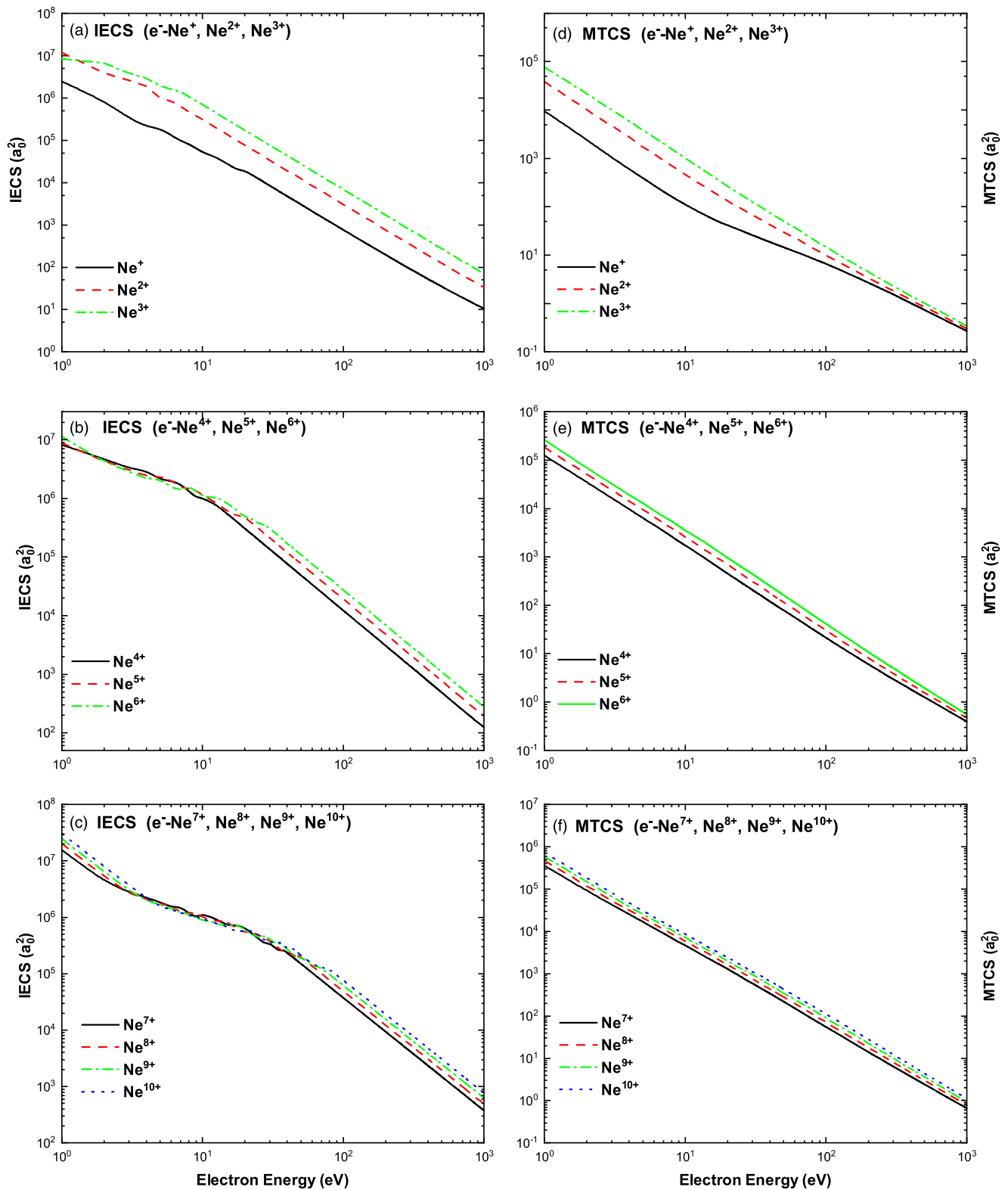



Fig. 14. (Color online) Energy dependence of IECs and MTCSs for the elastic scattering of electrons from $\text{Ne}^+ - \text{Ne}^{10+}$.

Acknowledgments

We greatly acknowledge the help in NSA calculations and useful suggestions of Dr. D. H. Jakubassa-Amundsen, Mathematics Institute, University of Munich, 80 333 Munich, Germany. M. Alfaz Uddin is grateful to University Grants Commission of Bangladesh for financial support. Mahmudul H

Khandker would like to thank University of Rajshahi for partial funding through project no-5/52/RU/Science-2/18-19.

ORCID iDs

Mahmudul H. Khandker  <https://orcid.org/0000-0001-9097-923X>

A. K. F. Haque  <https://orcid.org/0000-0002-1735-3967>

- 1) F. Salvat, A. Jablonski, and C. J. Powell, "Elsepadirac partial-wave calculation of elastic scattering of electrons and positrons by atoms, positive ions and molecules," *Comput. Phys. Commun.* **165**, 157 (2005).
- 2) M. I. Hossain, A. Haque, M. Atiqur, R. Patoary, M. Uddin, and A. Basak, "Elastic scattering of electrons and positrons by atomic magnesium," *Eur. Phys. J. D* **70**, 41 (2016).
- 3) S. Brotton, P. McKenna, G. Gribakin, and I. Williams, "Angular distribution for the elastic scattering of electrons from $\text{Ar}^+(3s23p52p)$ above the first inelastic threshold," *Phys. Rev. A* **66**, 062706 (2002).
- 4) A. Müller, "Fundamentals of electron-ion interaction," *Hyperfine Interact.* **99**, 31 (1996).
- 5) S. Khare and D. Raj, "Critical points for elastic scattering of electrons by light atoms," *J. Phys. B: At. Mol. Phys.* **13**, 4627 (1980).
- 6) M. Dapor, "Polarized electron beams elastically scattered by atoms as a tool for testing fundamental predictions of quantum mechanics," *Sci. Rep.* **8**, 5370 (2018).
- 7) K. Kollath and C. Lucas, "The critical position for elastic electron scattering in neon," *Z. Phys. A* **292**, 215 (1979).
- 8) D. Walker, "Relativistic effects in low energy electron scattering from atoms," *Adv. Phys.* **20**, 257 (1971).
- 9) A. C. Yates, "Spin polarization of low-energy electrons scattered elastically from atoms and molecules," *Phys. Rev.* **176**, 173 (1968).
- 10) R. Gulley, D. Alle, M. Brennan, M. Brunger, and S. Buckman, "Differential and total electron scattering from neon at low incident energies," *J. Phys. B* **27**, 2593 (1994).
- 11) D. Brewer, W. Newell, S. Harper, and A. Smith, "Elastic scattering of low-energy electrons by neon atoms," *J. Phys. B: At. Mol. Phys.* **14**, L749 (1981).
- 12) D. Register and S. Trajmar, "Differential, integral, and momentum-transfer cross sections for elastic electron scattering by neon: 5–100 eV," *Phys. Rev. A* **29**, 1785 (1984).
- 13) J. Williams and A. Crowe, "The scattering of electrons from inert gases. II. absolute differential elastic cross sections for neon, krypton and xenon atoms," *J. Phys. B: At. Mol. Phys.* **8**, 2233 (1975).
- 14) J. P. Bromberg, "Absolute differential cross sections of electrons elastically scattered by the rare gases. I. small angle scattering between 200 and 700 eV," *J. Chem. Phys.* **61**, 963 (1974).
- 15) R. DuBois and M. Rudd, "Differential cross sections for elastic scattering of electrons from argon, neon, nitrogen and carbon monoxide," *J. Phys. B: At. Mol. Phys.* **9**, 2657 (1976).
- 16) S. Gupta and J. Rees, "Differential cross sections for the elastic scattering of electrons by neon," *J. Phys. B: At. Mol. Phys.* **8**, 417 (1975).
- 17) R. Jansen, F. De Heer, H. Luyken, B. Van Wingerden, and H. Blaauw, "Absolute differential cross sections for elastic scattering of electrons by helium, neon, argon and molecular nitrogen," *J. Phys. B: At. Mol. Phys.* **9**, 185 (1976).
- 18) W. Kauppila, C. Kwan, D. Przybyla, S. Smith, and T. Stein, "Positron-inert-gas-atom elastic dcs measurements," *Can. J. Phys.* **74**, 474 (1996).
- 19) E. Knight, R. Singhal, R. Arthur, and M. Macauley, "Elastic scattering of electrons from 20, 22 Ne," *J. Phys. G: Nucl. Phys.* **7**, 1115 (1981).
- 20) F. De Heer, R. Jansen, and W. Van der Kaay, "Total cross sections for electron scattering by Ne, Ar, Kr and Xe," *J. Phys. B: At. Mol. Phys.* **12**, 979 (1979).
- 21) A. Robertson, "The momentum transfer cross section for low energy electrons in neon," *J. Phys. B: At. Mol. Phys.* **5**, 648 (1972).
- 22) J. Nickel, K. Imre, D. A. Register, and S. Trajmar, "Total electron scattering cross sections. I. He, Ne, Ar, Xe," *J. Phys. B: At. Mol. Phys.* **18**, 125 (1985).
- 23) A. Zecca, S. Oss, G. Karwasz, R. Grisenti, and R. Brusa, "Absolute total cross section measurements for intermediate energy electron scattering: III. Ne and Ar," *J. Phys. B: At. Mol. Phys.* **20**, 5157 (1987).
- 24) R. Wagenaar and F. de Heer, "Total cross sections for electron scattering from Ne, Ar, Kr and Xe," *J. Phys. B: At. Mol. Phys.* **13**, 3855 (1980).
- 25) G. Garcia, F. Arquerros, and J. Campos, "Total cross sections for electron scattering from Ne, Ar and Kr in the energy range 70–6000 eV," *J. Phys. B: At. Mol. Phys.* **19**, 3777 (1986).
- 26) A. Salop and H. Nakano, "Total electron scattering cross sections in O_2 and Ne," *Phys. Rev. A* **2**, 127 (1970).
- 27) B. Bransden and P. Hutt, "Electron and positron scattering by helium and neon," *J. Phys. B: At. Mol. Phys.* **8**, 603 (1975).
- 28) T. Griffith, G. Heyland, K. Lines, and T. Twomey, "Total cross-sections for the scattering of positrons by helium, neon, and argon at intermediate energies," *Appl. Phys.* **19**, 431 (1979).
- 29) W. Kauppila, T. Stein, J. Smart, M. Dababneh, Y. Ho, J. Downing, and V. Pol, "Measurements of total scattering cross sections for intermediate-energy positrons and electrons colliding with helium, neon, and argon," *Phys. Rev. A* **24**, 725 (1981).
- 30) A. C. L. Jones et al., "Positron scattering from neon and argon," *Phys. Rev. A* **83**, 032701 (2011).
- 31) H. Saha, "Low-energy elastic scattering of electrons from neon atoms," *Phys. Rev. A* **39**, 5048 (1989).
- 32) R. McEachran and A. Stauffer, "Elastic scattering of electrons from neon and argon," *J. Phys. B: At. Mol. Phys.* **16**, 4023 (1983).
- 33) W. Fon and K. Berrington, "The elastic scattering of electrons from inert gases. II. neon," *J. Phys. B: At. Mol. Phys.* **14**, 323 (1981).
- 34) F. Byron Jr. and C. J. Joachain, "Elastic scattering of electrons and positrons by complex atoms at intermediate energies," *Phys. Rev. A* **15**, 128 (1977).
- 35) M. E. Riley, C. J. MacCallum, and F. Biggs, "Theoretical electron-atom elastic scattering cross sections: selected elements, 1–256 keV," *At. Data Nucl. Data Tables* **15**, 443 (1975).
- 36) K. Baluja, A. Jain, H. Jones, C. Weatherford, and K. Karim, "Elastic differential cross sections for positron-neon scattering," *J. Phys. B* **24**, L93 (1991).
- 37) A. Kadyrov and I. Bray, "Recent progress in the description of positron scattering from atoms using the convergent close-coupling theory," *J. Phys. B* **49**, 222002 (2016).
- 38) H. Überall, "Electron scattering from complex nuclei (Academic, New York, 1971).
- 39) A. Haque, M. Haque, M. S. Hossain, M. I. Hossain, M. A. R. Patoary, M. Maaza, A. Basak, B. Saha, and M. A. Uddin, "A study of the critical minima and spin polarization in the elastic electron scattering by the lead atom," *J. Phys. Commun.* **2**, 125013 (2018).
- 40) D. Jakubassa-Amundsen, "Dwba theory for elastic scattering of polarized electrons from heavy unpolarized nuclei," *J. Phys. G: Nucl. Part. Phys.* **41**, 075103 (2014).
- 41) F. Salvat, J. Martinez, R. Mayol, and J. Parellada, "Analytical dirac-hartree-fock-slater screening function for atoms ($z = 1-92$)," *Phys. Rev. A* **36**, 467 (1987).
- 42) B. Bransden, M. McDowell, C. Noble, and T. Scott, "Equivalent exchange potentials in electron scattering," *J. Phys. B: At. Mol. Phys.* **9**, 1301 (1976).
- 43) N. Padial and D. Norcross, "Parameter-free model of the correlation-polarization potential for electron-molecule collisions," *Phys. Rev. A* **29**, 1742 (1984).
- 44) T. Koga, "Analytical hartree-fock electron densities for atoms he through lr," *Theor. chim. Acta* **95**, 113 (1997).
- 45) J. P. Perdew and A. Zunger, "Self-interaction correction to density-functional approximations for many-electron systems," *Phys. Rev. B* **23**, 5048 (1981).
- 46) A. Jain, "Low-energy positron-argon collisions by using parameter-free positron correlation polarization potentials," *Phys. Rev. A* **41**, 2437 (1990).
- 47) F. Salvat, "Optical-model potential for electron and positron elastic scattering by atoms," *Phys. Rev. A* **68**, 012708 (2003).
- 48) G. Staszewska, D. W. Schwenke, D. Thirumalai, and D. G. Truhlar, "Quasifree-scattering model for the imaginary part of the optical potential for electron scattering," *Phys. Rev. A* **28**, 2740 (1983).
- 49) F. Gross, *Relativistic Quantum Mechanics and Field Theory* (Wiley, New York, 2008).
- 50) J. Furness and I. McCarthy, "Semiphenomenological optical model for electron scattering on atoms," *J. Phys. B: At. Mol. Phys.* **6**, 2280 (1973).
- 51) M. H. Mittleman and K. M. Watson, "Effects of the pauli principle on the scattering of high-energy electrons by atoms," *Ann. Phys. (N.Y.)* **10**, 268 (1960).
- 52) N. F. Mott, Massey, and H. S. Wilson, *The Theory of Atomic Collisions* (Clarendon, Oxford, 1965) Vol. 35.
- 53) M. E. Rose, "Relativistic electron theory (Wiley, New York, 1961).
- 54) F. Salvat, J. Fernández-Varea, and W. Williamson Jr., "Accurate numerical solution of the radial schrödinger and dirac wave equations," *Comput. Phys. Commun.* **90**, 151 (1995).
- 55) J. Kessler, "Electron spin polarization by low-energy scattering from unpolarized targets," *Rev. Mod. Phys.* **41**, 3 (1969).
- 56) M. H. Khandker, A. Haque, M. Maaza, and M. A. Uddin, "Elastic scattering of electrons from the ions of argon isonuclear series," *Phys. Scr.* **94**, 075402 (2019).
- 57) K. Josphura and B. Antony, "Total (including ionization) cross sections of electron impact on ground state and metastable ne atoms," *Phys. Lett. A* **289**, 323 (2001).
- 58) K. Josphura and C. G. Limbachiya, "Theoretical total ionization cross-sections for electron impact on atomic and molecular halogens," *Int. J. Mass Spectrom.* **216**, 239 (2002).
- 59) H. De Vries, C. De Jager, and C. De Vries, *At. Data Nucl. Data Tables* **36**, 495 (1987).
- 60) D. Yennie, D. G. Ravenhall, and R. Wilson, "Phase-shift calculation of high-energy electron scattering," *Phys. Rev.* **95**, 500 (1954).

- 61) F. Gianturco, A. Jain, and J. Rodriguez-Ruiz, "Test of local model potentials for positron scattering from rare gases," *Phys. Rev. A* **48**, 4321 (1993).
- 62) J. Stepanek, "Electron and positron atomic elastic scattering cross sections," *Radiat. Phys. Chem.* **66**, 99 (2003).
- 63) A. F. Haque, M. A. Uddin, D. Jakubassa-Amundsen, and B. C. Saha, "Comparative study of ev to gev electrons and positrons scattering elastically from neutral atoms," *J. Phys. B* **51**, 175202 (2018).
- 64) H. Tolhoek, "Electron polarization, theory and experiment," *Rev. Mod. Phys.* **28**, 277 (1956).
- 65) D. Jakubassa-Amundsen, "Elastic scattering of spin-polarized electrons and positrons from ^{23}Na nuclei," *Nucl. Phys. A* **975**, 107 (2018).
- 66) B. Jhanwar, S. Khare, and A. Kumar Jr., "Elastic scattering of electrons on Ne atoms at intermediate energies," *J. Phys. B: At. Mol. Phys.* **11**, 887 (1978).
- 67) D. G. Thompson, "The elastic scattering of slow electrons by neon and argon," *Proc. R. Soc. London, Ser. A* **294**, 160 (1966).
- 68) I. McCarthy, C. Noble, B. Phillips, and A. Turnbull, "Optical model for electron scattering from inert gases," *Phys. Rev. A* **15**, 2173 (1977).
- 69) K. Blum and P. Burke, "Phaseshifts and differential cross sections for elastic electron-neon scattering," *J. Phys. B: At. Mol. Phys.* **8**, L410 (1975).
- 70) E. Krishnakumar and S. Srivastava, "Ionisation cross sections of rare-gas atoms by electron impact," *J. Phys. B* **21**, 1055 (1988).
- 71) B. Schram, F. De Heer, M. Van der Wiel, and J. Kistemaker, "Ionization cross sections for electrons (0.6–20 kev) in noble and diatomic gases," *Physica* **31**, 94 (1965).
- 72) D. Rapp and P. Englander-Golden, "Total cross sections for ionization and attachment in gases by electron impact. I. positive ionization," *J. Chem. Phys.* **43**, 1464 (1965).
- 73) D. Dewangan and H. Walters, "The elastic scattering of electrons and positrons by helium and neon: the distorted-wave second born approximation," *J. Phys. B: At. Mol. Phys.* **10**, 637 (1977).
- 74) P. L. Bartlett and A. T. Stelbovics, "Calculation of electron-impact total-ionization cross sections," *Phys. Rev. A* **66**, 012707 (2002).
- 75) S. Mori and O. Sueoka, "Excitation and ionization cross sections of He, Ne and Ar by positron impact," *J. Phys. B* **27**, 4349 (1994).
- 76) H. Knudsen, L. Brun-Nielsen, M. Charlton, and M. Poulsen, "Single ionization of H_2 , He, Ne and Ar by positron impact," *J. Phys. B* **23**, 3955 (1990).
- 77) F. Jacobsen, N. Frandsen, H. Knudsen, U. Mikkelsen, and D. Schrader, "Single ionization of He, Ne and Ar by positron impact," *J. Phys. B* **28**, 4691 (1995).
- 78) G. Laricchia, P. Van Reeth, M. Szluinska, and J. Moxom, "Total positron-impact ionization and positronium formation from the noble gases," *J. Phys. B* **35**, 2525 (2002).
- 79) J. P. Marler, J. Sullivan, and C. M. Surko, "Ionization and positronium formation in noble gases," *Phys. Rev. A* **71**, 022701 (2005).
- 80) R. McEachran, A. Ryman, and A. Stauffer, "Positron scattering from neon," *J. Phys. B: At. Mol. Phys.* **11**, 551 (1978).
- 81) S. Singh, R. Nagma, J. Kaur, and B. Antony, "Study of elastic and inelastic cross sections by positron impact on inert gases," *Eur. Phys. J. D* **72**, 69 (2018).
- 82) D. V. Fursa and I. Bray, "Convergent close-coupling method for positron scattering from noble gases," *New J. Phys.* **14**, 035002 (2012).
- 83) B. Srigengan, P. McKenna, P. McGuinness, and I. Williams, "Elastic scattering of electrons from argon ions," *Phys. Scr.* **1999**, 272 (1999).
- 84) C. Bélenger, P. Defrance, R. Friedlein, C. Guet, D. Jalabert, M. Maurel, C. Ristori, J. Rocco, and B. Huber, "Elastic large-angle scattering of electrons by multiply charged ions," *J. Phys. B* **29**, 4443 (1996).